Responses to Reviewer 1:

We thank the reviewer for a careful reading of the manuscript and helpful comments.

1. One burning question I had is whether the results would hold up for the much deeper open and closed cell cases found over the Southeast Pacific during VOCALS. The simulations in Wang et al. (2011) could be used here. The authors do experiment with the impact of PBL depth (section 4.3), but the PBL height difference in the contrasting case looks to be only about 100 m higher (Fig. 5b). The VOCALS cases were more like double the PBL depth.

Insights gleaned based on the Reviewer's other questions on the vertical stratification of the boundary layer (questions 2, 3, 5) shed some light on this question. We show in our responses below that the redistribution of TKE from predominantly top-down generated (closed cell) to bottom-up generated (open cell) is associated with both the duration and the magnitude of the N perturbation. Vertical mixing decreases with both duration and magnitude of the N perturbation and recovery therefore takes longer.

We concur that exploring recovery in a range of boundary layers, including much deeper ones, would be worthwhile. For now we believe that the insights gained from the vertical structure, and the existing test on a somewhat deeper boundary layer are sufficient to address this issue. (The current paper would need to be lengthened quite significantly if a rigorous analysis of a much deeper boundary layer were to be performed.)

We make it clear in the revised manuscript that the results pertain to a fairly shallow boundary layer and that recovery might change in deeper boundary layers. We surmise that recovery might be even slower in deeper boundary layers where the potential for vertical stratification is greater.

2. The authors do a good job explaining how the lagged recovery appears to relate to the difficulty establishing strong longwave cooling against precipitation losses. However, I wonder if the explanation is a little simplistic. To recover a closed cell state does not simply require LW cooling, but it requires that parcels cooled by LW cooling are able to sink under their buoyancy to a level whereby surface moistening can replenish the moisture supply to the cloud layer. I would therefore expect that the recovery timescale might also depend on the time that the PBL has been allowed to remain in a decoupled state (i.e., the time between N drop and N increase). An open cell PBL has a rather stratified upper PBL, so the LW cooling driving recovery will need time to drive efficient and deep mixing. The authors do not specifically mention this. It would be interesting to complete a sensitivity study where the low N period is either shortened or extended (perhaps both).

We now support our arguments with a number of different analyses.
i) We point to the fact that the cooling also has to overcome the stratification generated by the precipitation. (See Abstract, analysis around Fig. 7 and 8 and conclusions).This

issue is to some degree addressed by using smaller perturbations to N, which result in weaker rainrates, and therefore weaker stabilization. It is also addressed by the analysis of the vertical TKE profiles in response to question 3.

ii) We have performed simulations with both shorter and longer duration N perturbation to explore this issue. Instead of a 4 h open cell duration we have experimented with 2 h 6 h, and 8 h durations (figure below).

Clearly the asymmetry in LWP manifests at all durations of perturbation, and is commensurate with the duration. This is in agreement with the lower precipitation rates caused by the weaker perturbations to N already shown in Figure 3. In the revised text we tie these issues together more carefully.

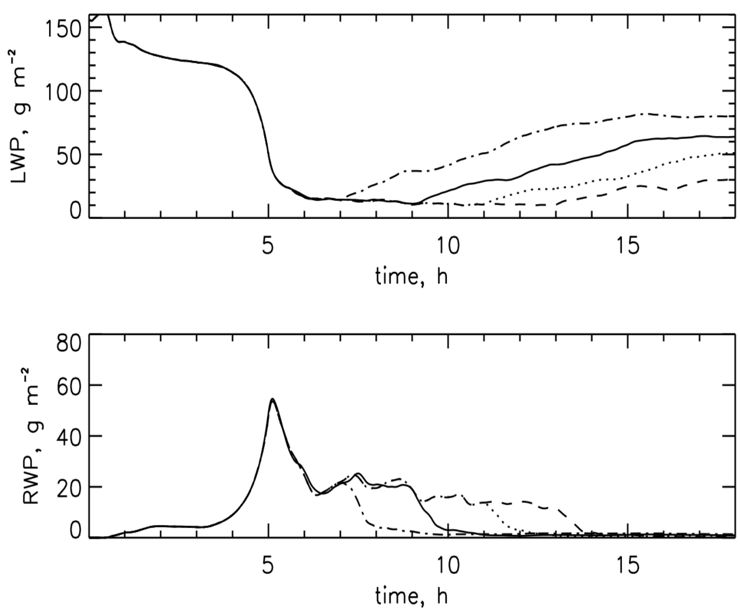

Figure: LWP and RWP time series for a 4h (solid line, as in Fig. 3), 6 h (dotted line), 8h (dashed line), and 2 h (dashed-dotted line). The change in N is 90/mg to 5/mg.

iii) We have analysed vertical profiles of TKE and buoyant production of TKE and found that in the transition from open to closed cellular convection, recovery is hampered by a layer of buoyancy consumption of TKE at roughly 300 m altitude, associated with the rain that persists into recovery. It is only after this region of buoyancy consumption peters out that the total water vapour flux can increase sufficiently so as to resupply moisture to the cloud.

A new Fig. (8) (see temporary snapshots below) is added and addressed along with Fig. 7. Note that we analysed a number of our other results and all point to this region of buoyancy consumption of TKE. There is also a clear relationship between the rate of recovery and the magnitude, and temporal and physical extent of the region of buoyancy consumption.

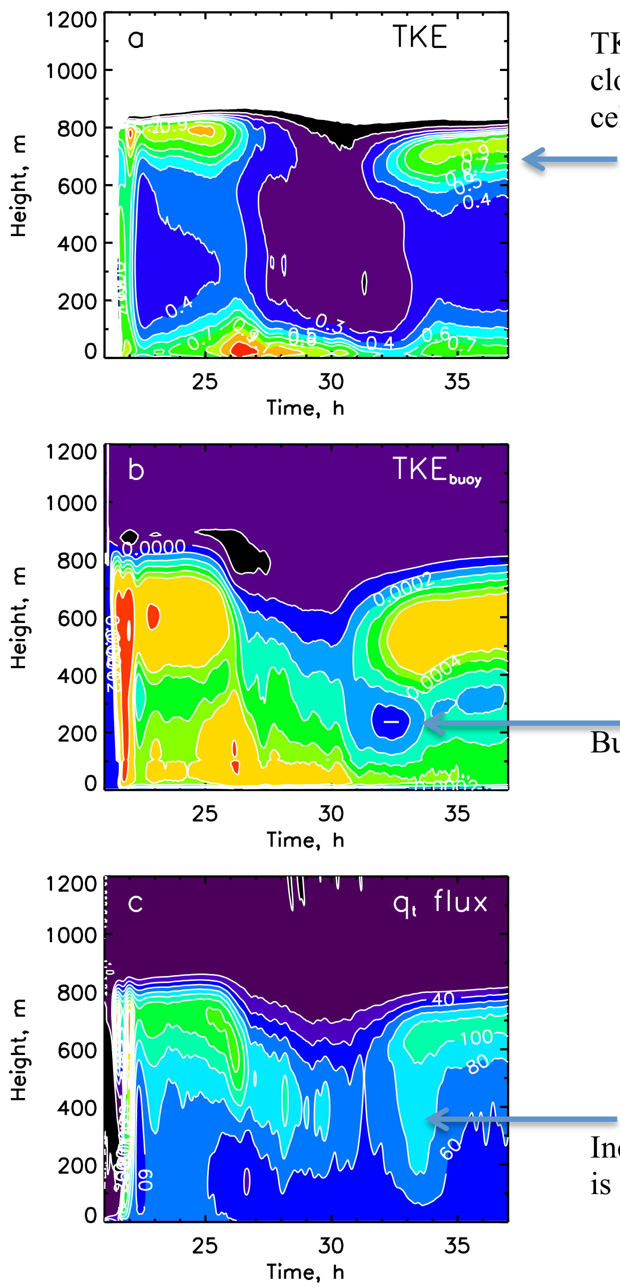

TKE in cloud layer transitioning to surface during closed-to-open transition. Low TKE state during open cell state

Buoyancy consumption of TKE

Increase in qt flux after buoyancy consumption of TKE is significantly reduced.

3. In my view, the connections between TKE and LW cooling need to be explored further. Can the authors show how different levels in the vertical contribute to the TKE and to its recovery. This would help strengthen the argument about a lack of reversibility. It might also explain why relatively small reductions in N seem to cause a more reversible transition, despite driving significant reductions in precipitation. What do the vertical profiles of theta and q look like during the transition?

TKE profiles are explored here for the standard GCSS case (Fig. 5).
We do this for two N perturbations (90→5→ 90/mg, left column and 90→35→90/mg, right column in figure below). One can clearly see how the larger N perturbation generates reduction in TKE over a deeper layer, along with weaker mixing in qt and thetal.

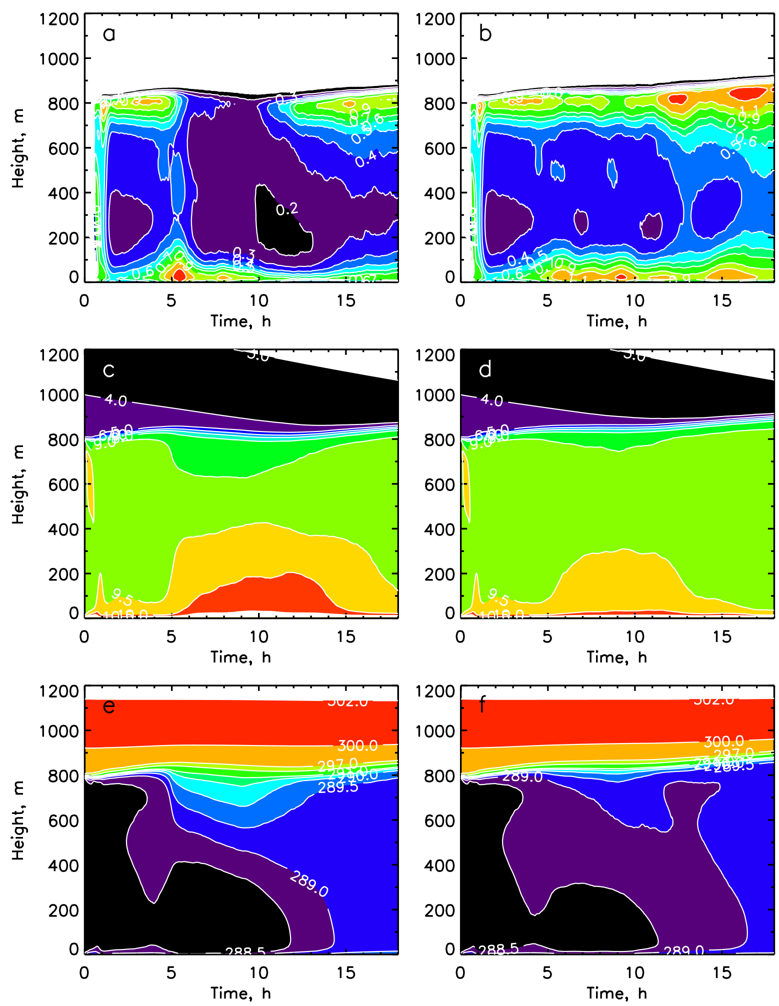

Figure: Profiles of (a, b) TKE, (c,d) qt and (e, f) thetal for left, the 90-to-5/mg perturbation (4 h) and right, the 90-to-35/mg perturbation (4 h).

We note that thetal and q profiles are shown in Fig. 5 for two of the cases (90→5→90/mg and no N perturbation) which already shows the reduction in vertical mixing associated with drizzle.

4. The predator-prey model results seem obvious to me, unless I am missing a subtlety. The authors essentially tune the rate of cloud building (tau1) and show that this affects the rate of cloud building (recovery). Why is this a surprise? The big question is what drives the slower recovery time. The predator-prey model, as far as I can tell, specifies this as an external parameter.

The reviewer is correct that the rate of recovery is an external parameter and that the predator-prey equations do not address *what* drives recovery.

The predator-prey analysis is now expanded. First we show results for different levels of Delta N, as in the CRM results. Secondly, we show results for more realistic tau_1 (3 h and 6 h). Thirdly, we discuss how the delay terms in the equations create an inherent asymmetry in the system.

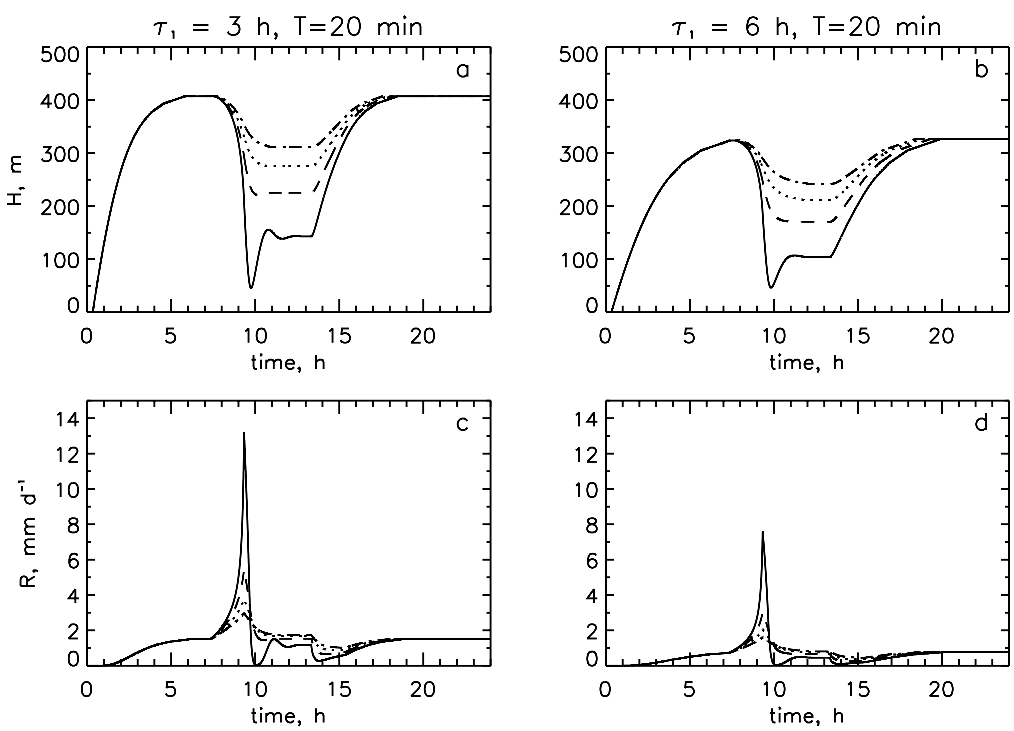

5. Figure 7. It is remarkable that during the period with the highest RWP (hour 25- 26), the TKE remains unchanged, and only reduces when the RWP falls from its peak value. Could the TKE be preserved despite significant precipitation because of cold pool formation?

The figures in response to questions 2 and 3 (above) serve to address this question. One can clearly see the shift from TKE maximum at cloud top during the closed cell period and the rapid shift to the surface upon transition to the open cell state (t ~ 5 h). See new Fig. 8 (above) for an example.

We show further analysis of the TKE and its contributions below.
We see how the TKE maximum shifts from a cloud top maximum in closed cell state followed by a rapid shift to a surface source on transition to the open state. The initial strong rain event drives strong surface TKE in the outflow, which slowly decays with time.

The TKE is broken into components: This analysis pertains to the analysis in current Fig. 7. All have the same color scale.

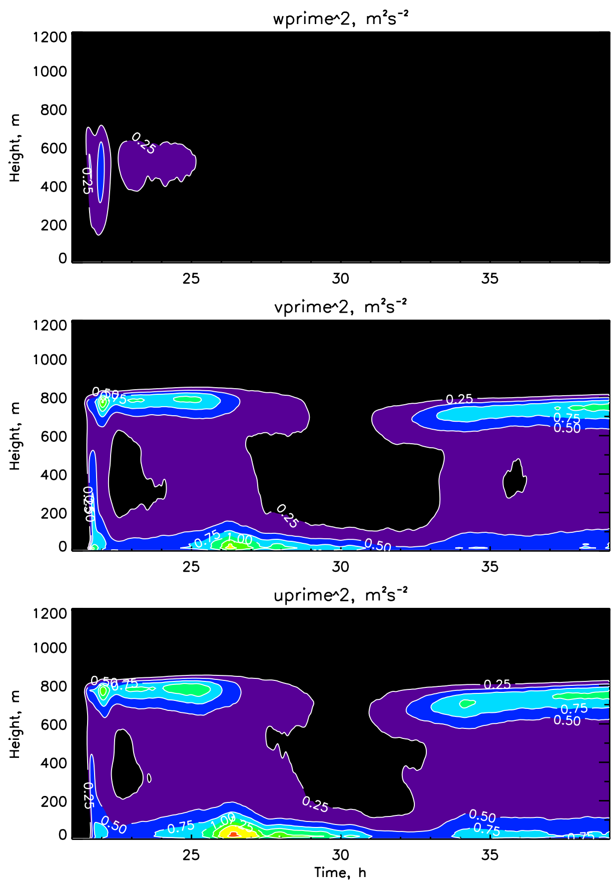

The heavily raining stage is one where cold pools form and maintain TKE through their interactions.

The new Figure 8 discussing the recovery mechanism show TKE, buoyancy production of TKE, and qt profiles to illustrate this point.

MINOR ISSUES:

1. P5555, line 10. Wood and Hartmann (2006) quantifies a number of important aspects of open and closed cells, including their aspect ratios, geographical distributions, meteorological situations etc.

Reference added as suggested.

2. P5560, line 23. What aspect of cloud formation is CCN limited? Are the authors referring to increased supersaturation and slowed condensation under low CCN conditions?

This was the intent. However because the model doesn't represent CCN we have reworded the text.

3. P5560, line 25. Didn't Pawlowska and Brenguier uncover a 1/N (not 1/sqrt(N) as stated here) dependence of precip on cloud drop concentration?

Agreed. Our original intent was to use a published relationship as an example but we now make this more general.

4. P5562, line 21-23. Subtropical marine stratocumulus tend to occur in regions with very dry free tropospheres, yet here we see recovery slowed down by entrainment of dry FT air. Thus, the statement that factors driving the rate of recover are the same as those driving cloudiness in general, seems to be a little questionable.

We now clarify this issue and revise the wording. We note that there are multiple aspects of a dry free troposphere that cannot easily be isolated. E.g., stronger radiative cooling (which enhances cloudiness) can be offset by entrainment (which may dilute cloud water). However, the latter depends on inversion strength and drizzle, amongst other factors.

5. Why are the times in Fig. 7 given as >20 hours? I thought the simulations were about 18 hours long.

The simulations starting at night that include shortwave forcing pass through midnight so that at t> 24 h, one needs to subtract 24 to get local time. Because there are occasions when simulations with and without shortwave radiation are compared (e.g., Fig. 11), we prefer to keep a simple time axis and alert the reader to this representation of time.

6. Section 4.2. Do the simulations with a dry FT in this section allow the low moisture to impact the PBL moisture budget upon entrainment?

No. This is stated in the original text.

7. Section 4.4. I didn't understand the significance of the mean vs variability LWP phase space. This seems to connect with another paper, but what is the point of showing it here?

The point is to show yet another aspect of the asymmetry, namely one in which the relative dispersion of the "recovered" closed cell state is characterized by higher relative dispersion in LWP for a given mean LWP. An example is the use of such relationships in the CLUBB parameterization.

Responses to Reviewer 2:

We thank the reviewer for a careful reading of the manuscript and for helpful comments.

Specific comments

1. Abstract: "Sysyphusian" is not a word. Perhaps the authors meant "Sisyphean"? But that term refers to a task that cannot be completed, which does not apply here because (a) there is no agent performing a task here, and (b) the system does completely recover from the open cellular convection. I would use a term that is consistent with the study's findings, instead.

The reviewer is correct. We should have used Sisyphean. Regarding whether the task can indeed be completed depends on the circumstances (e.g., in Fig. 7c the trajectory in LWP; TKE space is not closed and so strictly speaking full recovery has not occurred.). The term was intended to contrast between the runaway effect for the closed to open transition and the relative difficulty of recovery. Nevertheless, given a desire to appeal to a broad readership that may not have been exposed to these narratives, we remove the term.

2. p 5556, l 22: The claim that avoiding aerosol entirely and instead directly controlling cloud droplet concentrations, "allows a more direct assessment of the importance of the rates of aerosol removal and replenishment" does not make sense and needs clarification. How is it that bypassing aerosol completely allows for assessment of aerosol sinks and sources (which are never assessed)? This sentence would make sense if "does not" were inserted before "allows".

The reviewer is correct. “allows” is changed to “avoids”

3. p 5557, l 5: I would say "SAM solves the anelastic equations" or so rather than the confusing statement that "SAM is an anelastic system". Note that it also provides an option to solve the Boussinesq equations for shallow convection in LES mode according to the paper cited.

Changed as suggested.

4. p 5557 l 16: "Grid size" should be replaced with "Grid spacing" or so and "smaller...grids" should be replaced with "finer...grids" or so, since the term "small grid" and "grid size" describe the size of a grid, not mesh refinement.

Changed as suggested

5. p. 5558, l 9: "Rainrate" is not a word. Also, is the rain rate defined at the surface or cloud base or what?

We suspect that different journals have their respective spelling preferences. We have changed rainrate to rain rate but leave this to the technical editor to decide.

The rainrate in the predator-prey model is a system rainrate that is not vertically resolved. This is now clarified.

6. p. 5559, l 17: The notation "m g^-1" means "meters per gram" where the authors certainly intended "mg^-1", meaning "per milligram". This notational error pervades the text and figure captions.

Thank you for catching this. The original used mg^-1 and the space between m and g was added during the ACPD typesetting stage.

7. p 5560, l 5: Given that LWP includes cloud water and rainwater, the modifier "cloud" before "liquid water" should be omitted.

Actually the liquid water path shown is just the cloud part, which is why the modifier was used.

8. p 5560, l 16: The term "commensurate" does not fit here. "Incommensurate" would be closer to what is being described, but I'd rephrase and pick another term entirely.

We are not sure why because the larger the imposed reduction in N, the larger the asymmetry. Therefore "commensurate" is appropriate.

9. p. 5560, l 23: "Cloud formation is CCN-limited" seems odd here, since there are no CCN in the simulations and clouds apparently form just fine in the simulations even at extremely low cloud droplet concentrations of 5/mg. Some rephrasing or omission is needed.

The text is rephrased. We note that at these very low N, the interacting outflows seem to be important for cloud maintenance.

10. p 5560, l 25: It is stated that R goes as LWP^1.5/sqrt(N) as if that were some universally-accepted relationship. It's not. It might be interesting to show how the results here compare with that relationship, though.

Agreed. Our intent was to use one common expression but we know generalize.

11. p. 5560, l 27: I would define ambiguous terms upon their first mention, such as f_c, z_i, and z_b, which can be defined in many ways. I would provide the definitions used in the analysis here.

The criteria used for these calculations are now defined.

12. p. 5561, l 18: The "left panel" is referred to but there are three of them. Perhaps "left column of panels"?

Changed to "left column".

13. p. 5561, l 19: It would be helpful to note after stating that the cloud layer warms that one can figure that out by noticing that theta_l is steady while q_l decreases, which implies that theta must have increased.

Noted as suggested.

14. p. 5561, l 21: The interpretation seems to imply that the 9.5 g/kg isosurface marks the top of the near-surface layer. The thinking is unclear.

It was not our intent to claim that the 9.5 g/kg isosurface marks the top of the near surface layer. We have now clarified the text.

15. p. 5562, l 6: "Largescale" is not a word.

We leave it to the technical editing phase to sort this out.

16. The first paragraph of Section 3.2, which is attempt to explain the relationship between LWP, precipitation, and TKE, could use a good bit more attention and clarification so that it becomes clear and that physical understanding is effectively conveyed.

This is now done in the revised version.

17. p. 5563, l 1: Conceptual elements are missing from the assertion that precipitation reaching the surface cools the surface and warms the cloud layer, because the statement does not make sense as presented.

The text is rewritten to explain this more fully.

18. p. 5563, l 8: When stating "LWP drives production of TKE" it would be helpful to note that there is a positive feedback at work in which TKE also supports LWP.

Added as suggested.

19. p. 5563, l 10: It would be helpful to explain why there is a roughly 1-h delay between LWP decreasing and the drop in TKE.

We now add a Figure (new Figure 8) to address this. We have analysed vertical profiles of TKE, buoyant production of TKE, and qt flux

Below is the new Fig. 8. First, one sees a clear shift in the TKE from the cloud to the surface associated with the transition from closed to open-cell state. The surface TKE is stronger for the more strongly precipitating case. It is this surface peak that contributes to boundary layer TKE and accounts for the delay. Second, in the transition from open to closed cellular convection, recovery is hampered by a layer of buoyancy consumption of

TKE at roughly 250 m altitude, associated with the rain that persists into recovery. It is only after this region of buoyancy consumption of TKE peters out that the total water vapour flux can increase sufficiently so as to resupply moisture to the cloud. We analyzed various other runs with different rates of recovery and showed that recovery is related to the extent, duration, and magnitude of this region.

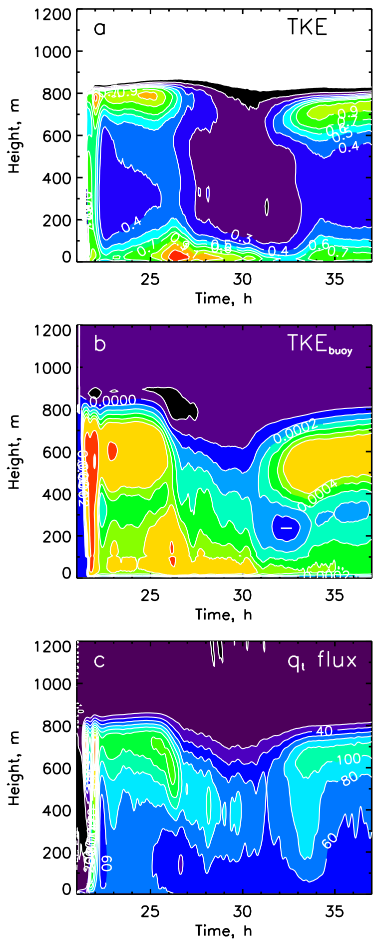

The figures below (not included in the revised text) break the TKE into its contributions and show how the cold-pools contribute to TKE.
The initial strong rain event drives strong surface TKE in the outflow, which slowly decays with time.

Figure below: TKE broken into components: This analysis pertains to the analysis in current Fig. 7. All have the same color scale.

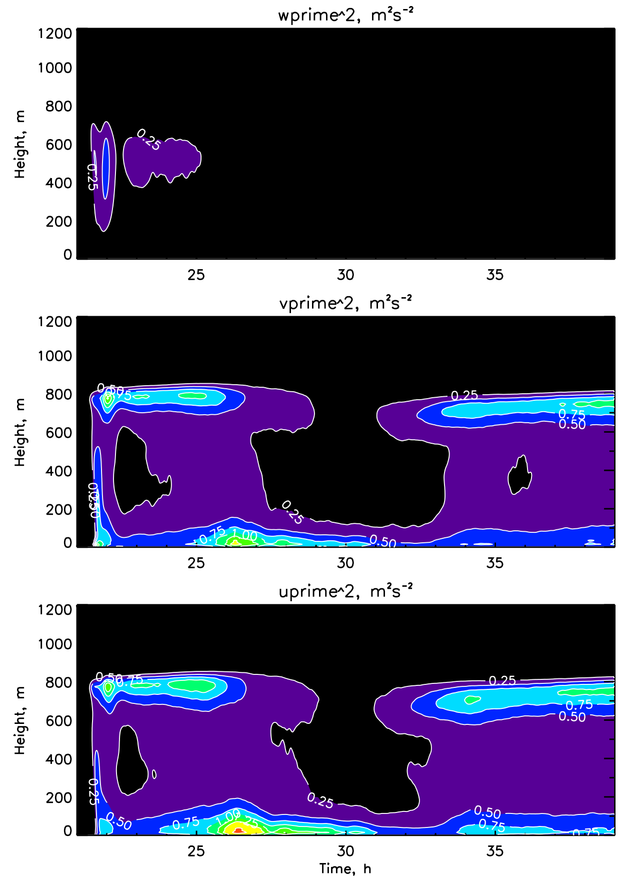

20. p. 5553, l 17: It is stated that the phase space trajectory "nicely" shows a limit cycle, but it does not. The very essence of a limit cycle is that a trajectory is closed, but the trajectory that is shown is open. High concepts are great, in principle, but readers may question their value when casual inspection reveals that they don't actually fit the evidence provided.

The reviewer is correct. We change the text to ".. nicely demonstrated as a plot in LWP, TKE phase space".

21. Section 3.2.2: It is unclear why the authors choose to increase the surface sensible heat flux with a goal of accelerating recovery. Increased sensible heat flux should reduce the relative humidity of the boundary layer and instead of generating thicker cloud, as mentioned on line 13, should generate thinner cloud, no? Or another angle – the authors seem to understand that increased radiative cooling is needed for the system to recover. Increased radiative cooling is removal of sensible heat from the system, working in the opposite direction of a "strong influx of energy" mentioned on line 8. So it seems to me that the entire notion of attempting to accelerate recovery by adding sensible heat is backwards, and it should only serve to slow down recovery.

First, as stated in the text, both sensible and latent heat fluxes are increased (maintaining the same Bowen ratio). Therefore increasing the fluxes will not necessarily result in thinner cloud.
Second, adding surface heating drives stronger turbulence as does increasing cloud top cooling.
Our point was to show that an added source of heat and moisture (dynamical forcing) could aid the recovery. We understand that this was not clearly laid out and have revised the text.

As an extra check, we also reran this simulation with a doubling of only the latent heat fluxes and achieved essentially the same result. There is one distinct difference however: when doubling only LH, the period of recovery to closed cell state is characterized by much more frequent shallow convection with low cloud base.

22. p. 5564, l 15: It is stated that "higher SH and LH are typically as [sic] drivers of open-cell formation" but aren't changes in sensible and latent heat fluxes the result of other changes associated with open-cell circulations, rather than drivers? Otherwise, open cells could be generated by simply increasing SH and LH fluxes. Can they? Furthermore, if higher latent heat fluxes are drivers of open-cell formation, how does that conform with open cells being associated with lower latent heat fluxes in fig 4b?

We agree that this section was not clearly laid out and it is now revised. Indeed, the cold pools associated with the raining period reduce LH and increase SH. We have revised the text in numerous places to address this point.

23. The foregoing issues regarding surface heat fluxes also appear in the abstract and conclusions.

Changes are made.

24. Section 4.1 contributes no understanding to this reader and the manuscript would benefit from omitting it. Either that or it needs to be fleshed out and tied into the rest of the study in a manner that adds value and conveys understanding.

The revised manuscript has a more thorough investigation of the predator-prey response. We now show results for the same range of N(t) as in the CRM results and show similar recovery characteristics. We contrast two time scales for recovery (3 h and 6 h) and show the impact on recovery. Note that both of these timescales produce reasonable (system average) rainrates (1-2 mm/day). We also discuss how the delay terms in the equations create an inherent asymmetry in the system.

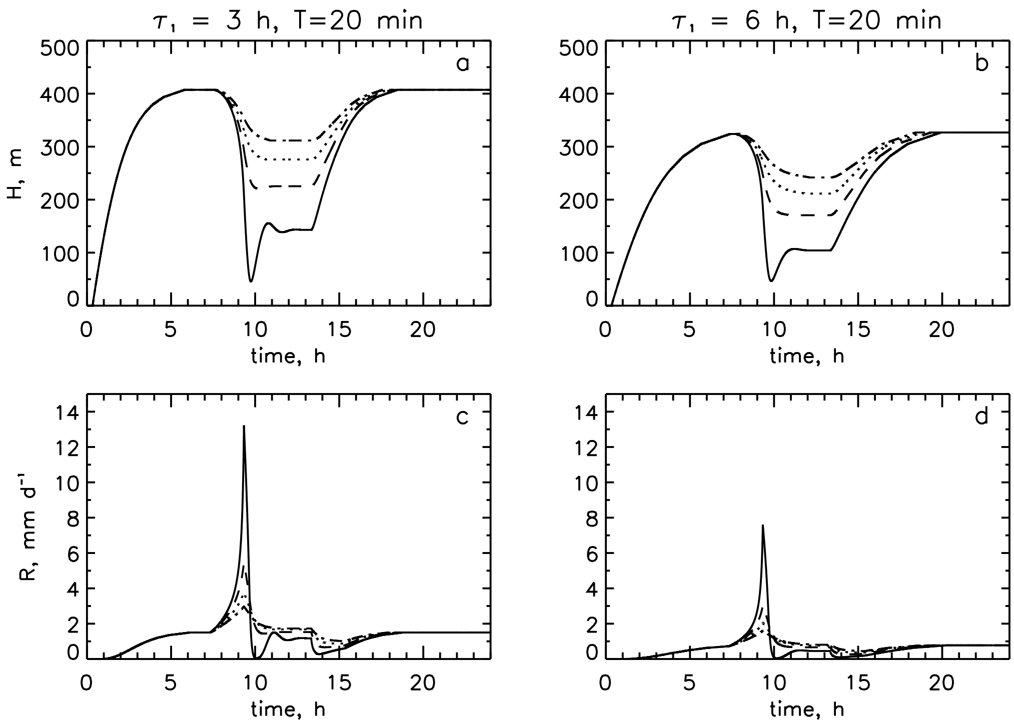

25. The rain rates for the predator-prey model seen in fig 9 are greater than those for the CRM by orders of magnitude, yet this is never even noted, let alone remarked upon. Seems like the dynamic regime of the predator-prey model is very different from that of the CRM simulations. Given such an adjustable model, the authors should either adjust it to be consistent with the CRM simulations or explain why that is impossible.

The revised manuscript presents predator-prey results that have similar rainrates. Nevertheless, we do stress that the goal of the simple system is to mimic behavior rather than exact values.

26. Section 4.2: The authors' understanding of the purpose of Beer's law longwave parameterization does not make sense to me. The reason it is used in model intercomparisons is to reduce possible sources of discrepancy between models, which typically use different radiative transfer schemes. The notion implied here that the Beer's law treatment represents an alternative treatment to real radiative transfer is very much off-target. The Beer's law treatment provides a small number of adjustable parameters that Larson et al. (2007) have shown allow it to reproduce the heating rates from real radiative transfer models. So if the authors find that the Beer's law formulation does not produce heating rates that are comparable to those with their radiative transfer model, that just shows that the authors failed to tune the adjustable parameters so that the rates are comparable. Used properly (which means tuning the adjustable parameters to reasonably match the heating rates given the conditions input to a real radiative transfer model), the only disadvantage of a Beer's law formulation in this context is that it is not *set up to readily compute solar heating. It should be stated that such an extension would not be difficult, and the reasoning for not doing so provided.*

We agree with the reviewer. The text is now changed to reflect this point. We do note that it is fortuitous that the (un-tuned) Beer's Law treatment generates weaker cooling than the RRTM because it allows us investigate the role of the radiative cooling in the recovery.

27. The authors' claim that there may be some biases for the Beer's law formulation for broken clouds, even though it is being used with the independent column approximation. But RRTM is also being used with the same approximation. Why would there be any bias if both approaches are using the same treatment to treat horizontal heterogeneity?

The reviewer is correct. The text is changed.

28. Instead of, or in addition to, stating the specific humidity used for the free troposphere in RRTM, it would be helpful to provide the overlying column of water vapor, which is more physically relevant.

This is now added to the figure caption along with the details of the profile.

29. Appendix: "Grid size" should be "grid spacing" or so. Also, it should be stated whether or not the domain size is fixed for these tests.

Changed and clarified as suggested

30. Panel labels are far too small in fig 2.

Labels are increased as suggested.

31. The surface precipitation rate shown in fig 3 is about a factor of five smaller than the average value measured in the open-cells for this case. This discrepancy should be noted and the implications discussed.

The original figure showed the domain-average rainrate. The revised figure shows the rainrate averaged over precipitating areas with a threshold rainrate of 0.1 mm/day in addition to the mean value. This accounts for the factor of 5 identified by the reviewer. Both timeseries are of interest but we now show the conditionally averaged ones.

32. There is a units problem in the equation provided in the fig 6 caption.

The text is changed to clarify the units.

33. The "domain and boundary-layer average" mentioned in the fig 7 caption is confusing. Surely the domain is deeper than the boundary layer, so this description does not make sense.

The average was done over the boundary layer, both horizontally and vertically. This is now clarified.

34. The legend, which appears to show grid sizes (numbers without units would seem to indicated that what is referred to is the number of grid cells), evidently conflicts with the description in the main text. A more complete figure caption might help.

This is now clarified and the legend and caption are changed to make it clear that grid spacings/lengths are in meters.

Manuscript prepared for Atmos. Chem. Phys.
with version 2014/07/29 7.12 Copernicus papers of the LaTeX class copernicus.cls.
Date: 4 June 2015

On the Reversibility of Transitions between Closed and Open Cellular Convection

Graham Feingold[1], Ilan Koren[2], Takanobu Yamaguchi[3,1], and Jan Kazil[3,1]

[1]Chemical Sciences Division, NOAA Earth System Research Laboratory (ESRL), Boulder, Colorado, USA
[2]Weizmann Institute, Rehovot, Israel
[3]Cooperative Institute for Research in Environmental Sciences, University of Colorado Boulder, Boulder, Colorado, USA

Correspondence to: Graham Feingold
(graham.feingold@noaa.gov)

Abstract. The two-way transition between closed and open cellular convection is addressed in an idealized cloud resolving modeling framework. A series of cloud resolving simulations shows that the transition between closed and open cellular states is asymmetrical, and characterized by a rapid ("runaway") transition from the closed- to the open-cell state, but slower recovery to the closed-cell state. Given that precipitation initiates the closed-open cell transition, and that the recovery requires a suppression of the precipitation, we apply an *ad hoc* time-varying drop concentration to initiate and suppress precipitation. We show that the asymmetry in the two-way transition occurs even for very rapid drop concentration replenishment. The primary barrier to recovery is the loss in turbulence kinetic energy (TKE) associated with the loss in cloud water (and associated radiative cooling), and the ~~stabilization~~ vertical stratification of the boundary layer during the open-cell period. In transitioning from the open to the closed state, the system faces the ~~Sisyphusian~~ task of replenishing cloud water fast enough to counter precipitation losses, such that it can generate radiative cooling and TKE. It is hampered by a stable layer below cloud base that has to be overcome before water vapor can be transported more efficiently into the cloud layer. Recovery to the closed cell state is slower when radiative cooling is inefficient such as in the presence of free tropospheric clouds, or after sunrise, when it is hampered by the absorption of shortwave radiation. Tests suggest that ~~a faster return~~ recovery to the closed-cell state ~~requires that the drop concentration recovery be accompanied by significant dynamical forcing, e.g., via an increase in surface latent and sensible heat fluxes. This is~~ is faster when the drizzle is smaller in amount, and of shorter duration, i.e., when the precipitation causes less boundary layer stratification. Cloud resolving model results on recovery rates are supported by simulations with a simple predator-prey dynamical system analogue. It is suggested that the observed closing of open cells by ship effluent likely occurs when aerosol intrusions are large,

when contact comes prior to the heaviest drizzle in the early morning hours, and when the free troposphere is cloud-free.

1 Introduction

Satellite imagery of cloud fields over the eastern edges of the oceanic basins exhibits both closed and open cellular cloud patterns that have captured the imagination of the atmospheric scientist and the layperson alike. Interest in these cellular cloud modes has been spurred by both the desire to understand these states, and to evaluate their consequences for shallow cloud reflectance and climate forcing. The closed cellular state is a mostly cloudy state characterized by broad, weak updrafts in the opaque cloudy cell center and stronger, narrower downdrafts around the cell edges. The open cell state is the “polar opposite” or “negative” in which narrow, strong, cloudy updrafts surround broad, weak downdrafts in the optically thin cell center. These states have been studied through observation (Sharon et al. 2006; Stevens et al. 2005; Wood and Hartmann, 2006; Wood et al. 2011) and modeling (Savic-Jovcic and Stevens 2008; Xue et al. 2008; Wang et al. 2009ab; Kazil et al. 2011, 2014; Yamaguchi and Feingold 2015), with most efforts addressing the closed to open cell transition. These studies have shown that rain is the likely initiator of the closed-to-open cell transition, pointing to the importance of deepening of the cloud (Mechem et al. 2012) and/or reduction in the cloud condensation nucleus (CCN) concentration. An interesting aspect of the precipitating open cellular system is that strongly buoyant cloudy cells produce rain, which imposes local negative buoyancy perturbations. The cloud-rain cycles thus ~~creates a dynamic~~ create an adaptive open-cell state that constantly rearranges itself as clouds move through positive buoyancy (non precipitating) and negative buoyancy (precipitating) cycles (Feingold et al. 2010, Koren and Feingold 2013). The closed-cell state has, in contrast, a more rigid structure that maintains itself over many hours (Koren and Feingold 2013).

A relatively under-studied aspect of the system is the two-way transition from closed-to-open-to-closed cells, and will be the focus of the current work. The results pertain to what have been termed Pockets of Open Cells (POCs; Stevens et al 2005) or Rifts (Sharon et al. ~~2005~~2006) in which open cells periodically appear within a meteorological setting that promotes closed cellular convection. This work does not address the broader question of closed to open cell transitions due to a warming sea surface temperature as one moves westward from the stratocumulus-capped continental coastlines. While some modeling work has addressed the two-way transition between states (Wang and Feingold 2009b; Berner et al. 2013) and there exists ample visual evidence of ship tracks “filling in” cloudiness in open cell fields (e.g. Goren and Rosenfeld 2012), there remain open questions regarding the relative ease of the two transitions and the extent to which aerosol intrusions control this transition. For example, Wang and Feingold (2009b) perturbed a cloud resolving simulation of the open cell state with a very large aerosol perturbation, and while a thin layer of cloud did fill the open cells, the aerosol was unable to convert the system to a closed state, presumably because the cloud was too thin to generate sufficient radiative cooling. The juxtaposition of these simulations and the observations ~~suggest~~ suggests that differences in meteorological conditions, aerosol perturbations, and the timing within the diurnal cycle might matter (Wang et al. 2011). The latter study explored other important factors such as the amount and distribution of the aerosol perturbation (in the form of shiptracks).

To address this problem, we use a cloud resolving atmospheric model that uses a simple microphysical scheme with an *ad hoc* control over the drop concentration and therefore, all else equal, the rain production. This is in contrast to our earlier work (Kazil et al. 2011) where the aerosol lifecycle was simulated from new particle formation through wet scavenging, and to more recent two-dimensional, multi day simulations of closed and open cell systems (Berner et al. 2013). The choice of a simple control over drop concentration ~~allows~~ avoids a more direct assessment of the importance of the rates of aerosol removal and replenishment. Supporting simulations are also performed using a dynamical systems analogue to the aerosol-cloud-precipitation system in the form of modified predator-prey coupled equations (Koren and Feingold 2011; Feingold and Koren 2013; Jiang and Wang 2014), which provides insight to the essence of the system, at minimal computational cost.

2 Model Description

2.1 Cloud System Resolving Model (CRM)

We use the System for Atmospheric Modeling (SAM) as described in Khairoutdinov and Randall (2003) with a 2nd order centered scheme for momentum advection and a monotonic 5th order scheme for scalar advection (Yamaguchi et al. 2011). SAM ~~is an anelastic system, which solves the~~ solves the anelastic Navier-Stokes equations on an Eulerian spatial grid. Prognostic equations are solved for liquid water static energy, mixing ratios of water vapor, cloud water, and rain water, and subgrid scale turbulence kinetic energy. While our earlier work used bin, or bin- emulating microphysics in LES and CRM (e.g., Feingold et al. 1996; Wang and Feingold 2009ab), the Khairoutdinov and Kogan (2000) microphysics is chosen here for expediency, and because its level of complexity is commensurate with the *ad hoc* specification of dN/dt.

The initial and boundary conditions follow the Second Dynamics and Chemistry of Marine Stratocumulus (DYCOMS-II RF02; Ackerman et al., 2009) but also include a number of perturbations. The domain is 40 km $\times$ 40 km wide and 1.6 km deep with a grid ~~size~~ spacing of 200 m in the horizontal and 10 m in the vertical. Tests with ~~smaller horizontal grids~~ finer horizontal grid spacings (100 m and 75 m) show that the key results are remarkably robust to the model grid ~~specification~~ spacing (Appendix A). The lateral boundary conditions are doubly periodic and the timestep is 1 s. Our base case is the standard Global Energy and Water Cycle Experiment (GEWEX) Cloud System

Study (GCSS) DYCOMS-II RF02 case with horizontal winds (*u; v* = 7.3; -3.5 m s^{-1} at 1000 m; see Ackerman et al. 2009) and an interactive surface model based on similarity theory; the large-scale subsidence is computed based on the large-scale horizontal wind divergence of 3.75 $\times$ 10^{-6} s^{-1}; longwave radiative flux divergence is calculated ~~based~~ using either on a simple liquid water path-dependent method (Ackerman et al., 2009) or the coupled Rapid Radiative Transfer Model (RRTM; Mlawer et al. 1997). Because of the shallow depth of the domain, a free tropospheric sounding is patched above the domain top for the RRTM radiation calculations. For the above-domain temperature sounding, we follow Cavallo et al. (2010). The domain top value of water vapor mixing ratio is used as the above-domain water vapor profile. Different domain-top values of water vapor mixing ratio will be considered in Section 4.2. While in principle, the simple longwave radiation scheme could be tuned to mimic that of RRTM (e.g., Larson et al. 2007), we have not done so. This has the salutary effect of providing different responses of radiative cooling to liquid water path, which will serve to elucidate sensitivity of transitions to longwave radiative cooling.

Simulations are on the order of 18 h so that some include significant periods of shortwave radiation. Perturbations to these initial and boundary conditions are shown in Section 3.1.4.

The second model is an adaptation of the the predator-prey model ~~applied to a cloud system~~ (Koren and Feingold, 2011). The model comprises three equations ~~for~~ that describe the cloud depth H, drop concentration N and ~~rainrate~~ rain rate R for the cloud system:

$$\frac{dH}{dt} = \frac{H_0 - H}{\tau_1} - \frac{\alpha H^2(t-T)}{c_1 N(t-T)}, \tag{1}$$

$$\frac{dN}{dt} = \frac{N_0 - N}{\tau_2} - c_2 N(t-T) R \tag{2}$$

and,

$$R(t) = \frac{\alpha H^3(t-T)}{N(t-T)}, \tag{3}$$

where c_1 is a temperature-dependent constant, and c_2 and α are constants based on theory. H_0 is the cloud depth that would be reached within a few timescales τ_1 in the absence of rain-related losses. Thus H_0 represents "meteorological forcing", or in population dynamics nomenclature, the "carrying-capacity" of the system. Similarly, N_0 is the drop (or aerosol) concentration "carrying-capacity" that the system would reach in a few τ_2 in the absence of rain. The N loss term on the right hand side of Eq. (2) captures a physically-based rate of removal. The delay T, represents the time required for cloud water to be converted to rainwater by collision and coalescence between drops~~($T \sim 15 - 20$ min)~~, and introduces significant complexity and nuanced response in the system of equations (Feingold and Koren, 2013). Here we substitute Eq. (2) with a simple time varying N similar to that imposed in the CRM simulations. ~~Rainrate~~ Rain rate is diagnosed from the prognostic variables H and N, again with delay T (Eq. 3). While the system of Equations (1 – 3) is represented by five primary parameters, H_0, N_0, τ_1, τ_2 and T, the use of a prescribed $N(t)$ instead of Eq. (2) reduces the free parameters to H_0, τ_1 and T . In the current work, we will select values of these parameters that are physically plausible, and/or that help illustrate the key points.

3 Results

3.1 Cloud Resolving Modeling

3.1.1 Time variation in N

A series of simulations with a prescribed evolution of drop concentration N is applied to all simulations (Fig. 1). The time series starts with a steady N = 90 mg^{-1} (equivalent to 90 cm^{-3} at an air density of 1 kg m^{-3}), which for the current case generates closed cell conditions with minimal precipitation. It then mimics the rapid drop in N associated with the runaway reduction in N in a developing open cell over the course of 2 h (e.g., Feingold et al. 1996; Wang and Feingold 2009a); a 4 h period of steady, low N; and then an equally rapid (2 h) rise in N back to pre-open cell conditions. Four different values of low N are applied: 5, 15, 25, and 35 mg^{-1}. The rapid rise back to 90 mg^{-1} is unrealistic given earlier work that estimated a recovery time of $\sim$ 10 h (Berner et al. 2013), but as will be shown, it provides a (near) upper bound on replenishment of the drop concentration, and anything less rapid serves to strengthen the arguments to be presented. The time series of N, specifically the recovery to $N = 90$ mg^{-1}, will be varied in a number of sensitivity tests.

3.1.2 Control Simulations

The control simulations use the GCSS specifications as described above, the simple longwave radiation scheme (no shortwave radiation) and surface latent and sensible heat fluxes that respond to the local surface horizontal winds. A series of snapshots of the cloud liquid water path (LWP) calculated from the modeled cloud and rain water mixing ratios (Fig. 2) shows an initial closed cellular state transitioning to an open cell state (distorted by the mean northwesterly flow), a filling in of cloud associated with the increase in N, which gradually provides colloidal and dynamical stability to the cloud, and finally, a more complete closed cellular cloud cover.

Figure 3 shows time series of the domain mean cloud LWP, rain water path (RWP) ~~, and~~ and surface rain rate R_{sfc}, and the mean surface rain rate ~~R~~conditionally sampled for $R_{sfc} \geq 0.1$ mm d^{-1} (R_{cond}). After the “spin up” of turbulence, by t = 3h the LWP is approximately steady at 110 g m^{-2} (although decreasing slowly). The reduction in N after 3 h results in rapid reduction in domain average LWP as rain ensues and cloud cover decreases, a period of relatively steady LWP – particularly for the low minimum N – and then a slow recovery after the increase in N at t = 9 h. In spite of the symmetry in the ramping down and up of N, there exists an asymmetry in LWP(t) commensurate with the ~~reduction in~~ minimum imposed value of N. Asymmetry also exists in RWP (t); initially strong RWP during the onset of drizzle ($t \approx 5$ h) is followed by a more steady but lower RWP (t = 6 – 9 h), and relatively steady ~~R~~R_{sfc}. This period is characterized by a balance between dynamical forcing that replenishes cloud liquid water, and by drizzle losses. Note that the start of the increase in N at 9 h does not put an immediate stop to rain, as evidenced by the long tail of low RWP and ~~surface rain rate R~~ R_{sfc} that persists even after N = 90 mg $^{-1}$ (t = 11 h). This is because ~~cloud formation is CCN-limited~~ in these very clean conditions ~~and initially~~ the increase in N initially helps to boost LWP, which further boosts rain. (Recall that $R \propto \mathrm{LWP}^{\cancel{1.5}\ \cancel{N^{-0.5}}\alpha}\ N^{-\beta}$; e.g., Pawlowska and Brenguier ~~2003.~~ 2003, with α approximately 3 $\times$ larger than β.)

~~The~~ Figure 4. shows the mean cloud fraction f_c (defined by a cloud liquid water mixing ratio q_c threshold of 0.01 g kg^{-1}), surface latent heat (LH) and sensible heat (SH) fluxes, inversion height z_i (based on the maximum gradient in liquid water potential temperature θ_l), and cloud base/top height (z_b/z_t ~~) are shown in Fig. 4.~~ ; calculated based on a q_c threshold of 0.01 g kg^{-1}). ($\theta_l \approx \theta - q_c\, L_v/c_{pd}$; with L_v the latent heat of vaporization and c_{pd} the specific heat of dry air at constant pressure.) Cloud fraction recovery is approximately symmetrical for high minimum N but becomes increasingly more asymmetrical as the minimum N approaches 5 mg^{-1}. Surface latent heat fluxes decrease, while sensible heat fluxes increase during the open cell period, consistent with the cooler and moister surface outflows (see e.g. Kazil et al. 2014 for more detailed analysis of the surface flux responses). The pre-open cell rise in cloud base and top height is suppressed during the raining period. Cloud bases for the different N perturbations all tend to converge after full recovery of N, while cloud tops for the stronger perturbations are up to $\sim$ 50 m lower. Note that because the calculations of z_t and z_i apply different criteria, the absolute values are somewhat different. The main point however is to compare the response to different $N(t)$.

3.1.3 No Aerosol Perturbation

It is of interest to compare these perturbed simulations to one in which there is no perturbation to N, i.e., N = 90 mg^{-1} for the entire simulation. Figure 5 shows profiles of total liquid water, total water mixing ratio q_t, and liquid water potential temperature θ_l for the control case and a simulation without any N perturbation. In the absence of a perturbation to N, the cloud does not produce substantial drizzle; even though the boundary layer deepens steadily, it does not produce enough liquid water to generate precipitation at N = 90 mg^{-1}, and it remains reasonably well-mixed. In contrast, the control simulation with a strong perturbation to N (5 mg $^{-1}$) exhibits significant drizzle-related reduction in cloud water and significant perturbation to the well-mixed state (Fig. 5, left ~~panel~~column). Notably, and in agreement with earlier studies (e.g., Stevens et al. 2005) the cloud layer dries and thus warms during the precipitating period while the surface cools and moistens. For example, this can be deduced from the fact that θ_l is steady while q_c decreases, which means that θ must have increased. By the end of the simulation, vertical mixing has increased; θ_l is approximately constant with height ~~but a moister near-surface layer~~. For q_t, vertical mixing also increases although a moister layer exists up to a depth of 100 m ~~persists, even though surface drizzle is < 0.01 mm day $^{-1}$ (Fig. 3c).~~ . Overall, however, the morphological structure of the cloud field, its flow structure (not shown) and the thermodynamic profiles at the end of the simulation, are consistent with a closed cellular system.

3.1.4 Sensitivity Tests

A number of sensitivity tests and perturbations to the initial and boundary conditions were performed to gauge robustness in the response to the $N(t)$ perturbation. These include (i) fixed surface fluxes (SH = 15 W m^{-2} and LH = 93 W m^{-2}); (ii) simulation of both shortwave and longwave radiation using RRTM; (iii) changing start times in the diurnal cycle; and (iv) varying free tropospheric humidity and largescale subsidence. This is just a subset of the various tests that could be performed. Figure 6 shows time series plots of LWP for these various tests. In all cases the asymmetry in LWP(t) in response to $N(t)$ is clear. Of interest is that RRTM tends to generate stronger longwave radiative cooling and therefore even in the presence of shortwave radiation, LWP recovery after the open-cell period is much more effective (c.f. Fig. 3a and Fig. 6b; see further discussions in Section 4.2). Delays in the start time of the simulation slow the LWP recovery (progressively weaker slopes with increasing delay in Fig. 6c) because of shortwave absorption, but once N has returned to 90 mg^{-1} the simulations converge. Other significant changes to the simulations are in response to changes in subsidence and free tropospheric humidity (Fig. 6d). A drier free troposphere (see Figure caption for details) reduces LWP during the first 4 hours of simulation, before the onset of drizzle. This reduction in LWP is magnified in the case of stronger subsidence but in the case of weaker subsidence, the loss in LWP is countered by the ability of the boundary layer to generate a deeper cloud. As might be expected, recovery to the closed cell state is slowest in the case of a dry free troposphere in combination with strong subsidence. Thus ~~the~~ meteorological conditions that ~~control~~ influence cloudiness itself set the stage for the rate of recovery after the drizzling period.

3.2 Relationship between Recovery, Turbulence Kinetic Energy and Convective Available Potential Energy

~~In stratocumulus,~~ Stratocumulus cloud water provides a source of ~~radiative cooling and generation of~~ longwave radiative cooling, which generates negative buoyancy and turbulence. Surface precipitation removes liquid water from the ~~system, cools the surface~~cloud layer and deposits it to the surface. Surface precipitation therefore reduces the amount of cooling associated with the evaporation of cloud water in the cloud layer, and warms the cloud layer~~, resulting in a more stable environment~~. Near surface evaporation of precipitation cools the surface layer. Thus surface precipitation serves to stabilize the boundary layer (e.g., Stevens et al. 1998). We therefore expect rain processes to manifest in TKE and Convective Available Potential Energy (CAPE). We analyze an illustrative case that includes a diurnal cycle (start time 21:00 LT) and a cycle of N from 90-to-5-to-90 mg^{-1} (Fig. 6b solid line). TKE is the grid-resolved component, averaged over the boundary layer depth. Sunrise is at approximately 06:00 LT, i.e., about the time of the beginning of N recovery. A time series of LWP, TKE, and CAPE reveals that during the initial closed cell phase (prior to t = 24 h), LWP drives production of TKE (Fig. 7ab), which in turn drives higher LWP. The prescribed drop in N results in precipitation and a loss of LWP. TKE also drops, but with a delay of approximately 1 h. This delay is associated with the surge in surface TKE on transition to the open cell state, associated with the surface outflows (Fig. 8a, $t \approx 27$ h). The surface TKE slowly wanes as the surface rain rate and outflows weaken. (The peak transitions back to cloud top upon recovery of the closed cell state at $t > 32$ h.) TKE continues to decrease during the open-cell, drizzling phase, and only begins to rebound approximately 1 h after the introduction of N, and the LWP recovery ~~.~~ (Fig. 7b). Later, LWP and TKE increase in unison and eventually peak simultaneously at maximum cloud recovery. During the last 4 h of the simulation, absorption of shortwave radiation results in a decrease in LWP. There is a steady decrease in CAPE over the course of the simulation~~(Fig. 7b)~~, which is also indicative of the inability of the system to rebound.

The asymmetry of the closed-open-close transition cycle is nicely demonstrated as a ~~limit cycle~~ plot in LWP, TKE phase space ~~.~~ (Fig. 7c). During the delay in TKE recovery upon reintroduction of N (t = 30 - 31 h), turbulence does not reinforce the LWP increase. Thus LWP recovery following the introduction of N is hampered by the inability of the system to generate turbulence via radiative cooling – itself a function of LWP.

Further analysis of the recovery shows that recovery is hampered by below cloud buoyancy consumption of TKE (Fig. 8 b) at $t \approx 32$ h and a height of ≈ 250 m (marked by a white minus sign on the figure). Analysis of other cases shows that this is a robust feature during the recovery stage, although it varies in magnitude and extent. Horizontal x-y slices through this region reveal that the buoyancy consumption of TKE is related to rising of cold air and sinking of warm air (e.g., Moeng 1987). (Figure not shown.) After the disappearance of this region of buoyancy consumption of TKE, the total water flux (vapor plus cloud water) into the cloud increases significantly (Fig. 8c, $t > 33$ h).

3.2.1 Influence of Rate of N replenishment on Recovery

Given the simplicity of the N representation, it is useful to consider whether recovery is limited by the rate of recovery of N at the end of the open-cell phase. Two variations on the control simulations (Fig.1, Fig. 3) are repeated. The first ramps N up from 5 mg^{-1} to 90 mg^{-1} within 5 min (as opposed to 2 h); the second ramps N up to 300 mg^{-1}, also within 5 min (Fig. ~~8~~9); both are highly unrealistic, considering the aerosol replenishment rates via new particle formation, mechanical surface production, and entrainment (Kazil et al. 2011). It is clear that even these unrealistically high N recharge rates make little difference in terms of the rate of increase in LWP and TKE. Small enhancements in recovery in f_c and deepening of the boundary layer are, however, evident. A more realistic N recovery rate of t= 10 h further delays recovery. Thus while the rate of replenishment ~~in~~ of N is clearly an important controlling factor for recovery, even immediate replenishment ~~in N~~ does not erase the asymmetry in the LWP and TKE recovery.

3.2.2 Influence of Meteorological forcing on Recovery

Given the close relationship between LWP and TKE – albeit with delay – we hypothesize that ~~a strong~~ an appropriately placed influx of energy and water into the system should help ~~with recovery.~~ recovery. There are various ways that this can be explored in modeling world but one straightforward way is by increasing surface sensible and latent heat fluxes which generate surface-driven buoyancy and moisture (e.g., Xue and Feingold, 2006). Another is through stronger cloud top cooling, which is explored in section 4.2. The control simulation is repeated, but this time the interactively calculated values of SH and LH are both increased by a factor of 2, coincident with, and following the beginning of the ramp up of N at 9 h. This is an *ad hoc* simulation, and is not meant to be tied to a specific scenario. As shown in Fig. ~~9~~10, recovery is significantly stronger. ~~Meteorological forcing of some kind, e. g. , in~~ This simulation also exhibits a layer of buoyancy consumption of TKE centered on $\sim$ 300 m during the recovery stage ($t > 10$ h for this case), as in Fig. 8b. However it is significantly weaker and diminished in size compared to the control case with standard interactive fluxes (figures not shown). Moreover, the ~~form of a propensity to generate thicker cloud, or an influx of boundary layer moisture, appear~~ q_t flux into the cloud layer is stronger and starts earlier in the recovery stage than for the control case. Thus the increased SH and LH help to reduce the strength, extent, and duration of this layer of buoyancy consumption of TKE, thereby accelerating recovery. An additional case in which only LH was doubled and SH was kept the same produced similar results vis-à-vis recovery in LWP during the open-to-closed cell transition, although there was a proliferation of shallow cumulus with low cloud base during this stage resulting from the lower lifting condensation level. Meteorological forcing that generates thicker cloud appears to be important for increasing the rate of LWP and TKE recovery, and transition back to the open cell state. ~~Note that although higher SH and LH are typically as drivers of open-cell formation, here the boundary layer has the propensity to generate closed cells, so that the stronger fluxes translate to stronger dynamical forcing. More detailed analysis of the relationship between surface fluxes and cell state can be found in Kazil et al. (2014).~~

4 Discussion

4.1 The Predator-Prey Model

~~Based on the results presented above, we apply~~ We explore the ability of the predator-prey ~~analogue to~~ model to capture key responses of the system to changes in N emanating from the ~~closed-open cell system , driven by a similar $N(t)$ as in the~~ CRM simulations~~, i. e.~~. To do so, we replace Eq. (2) with a time series much like that in Fig. 1 with high and low N values of 90 ~~mg $^{-1}$ and 10 mg $^{-1}$, respectively.~~ cm $^{-3}$ and 5, 15, 25 or 35 cm $^{-3}$, respectively. The transition times and the duration of the low N state are the same as in Fig. 1 however the time axis is shifted by 4 h to allow the model to spin up. (The low N state is reached at 9 h in these predator-prey calculations rather than 5 h as in Fig. 1.) Thus in keeping with the CRM simulations, we prescribe ~~the N~~ $N(t)$, which essentially overrides the replenishment time τ_2 ~~as well as~~ and prescribes two “carrying capacity” values N_0 = 90 ~~mg $^{-1}$ or 10 mg $^{-1}$~~cm $^{-3}$ or in the low N state, N_0 = 5, 15, 25, or 35 cm $^{-3}$. Other system parameters are H_0 = 650 m ~~, and~~ and microphysical delay T = 20 min. ~~Two predator-prey results , differing only in~~ The left column of Fig. 11 shows results for the meteorological forcing timescale τ_1 ~~(in~~ =3 h (Eq. 1) associated with “recharge” of liquid water (or cloud depth H)~~to the system, are shown in Fig. 10. One is a slow recharge time, τ_1 = 3 h and the other is a very short τ_1 = 0.5 h. For τ_1 = 3 h, the broad features of the LWP time series are similar to those produced by the CRM. This large τ_1 also exhibits slow LWP recovery following the~~ . It is apparent that the larger the imposed reduction in N, the larger is the decrease in H and the associated increase in R at the onset of heavy rain, much as in Fig. 3b. Thereafter, differences in R during the low H period are relatively small, again in agreement with Fig. 3b. However, we do note that for the 90 to 5 cm^{-3} simulation, R behavior is anomalous because of the overshoot to very low H (50 m) upon transition to very low N ~~, low LWP period. The short~~ caused by the large loss term in Eq. (1). The asymmetry in the H transitions is readily apparent, with larger reductions in N exhibiting stronger asymmetry, much as in the CRM.

The meteorological timescale τ_1 is now increased to 6 h (right column of Fig. 11), representing a slower rise to H_0 and is akin to a ~~strong meteorological forcingmuch like in Fig. 9 but~~ weaker external meteorological forcing. Weaker forcing can also be achieved by ~~increasing~~ decreasing H_0 ~~simultaneous with the~~ itself, but this can generate values of R that are unrealistic for stratocumulus and it is therefore more desirable to tune τ_1 for these exercises. For τ_1 = 6 h, the initial build-up in H prior to the N ~~recovery (results not shown)~~ perturbation is slower and the rain rates are weaker. The asymmetry in the transitions is even more pronounced. This is in broad agreement with Fig. 10, where it was shown that stronger forcing (in the form of higher surface fluxes) had a significant effect on recovery. ~~Decreasing τ_1 to 0.5 h significantly increases the rate of recovery of LWP, in agreement with Fig. 9. As with the CRM~~

Note that because of the existence of delay terms in Eqns. (1) and (3), one might *a priori* anticipate asymmetry in transitions for the imposed $N(t)$. For example, when transitioning from high H and high N (analogous to the closed state) to low H and low N (analogous to the open state), the source term for H is relatively small (because H is closer to H_0) and the loss term $(H^2(t-T)/N(t-T))$ is large. This explains the very rapid closed-to-open cell transition. When transitioning from low H and low N to high H and high N, the source term is relatively large but the loss term is also relatively large, particularly when the imposed $N(t-T)$ is small. This helps explain the slower recovery, as well as the dependence of the recovery time on the imposed minimum value of N.

Finally, as with the CRM results in Fig. 9, solution to the predator-prey equations with ~~very rapid~~ instantaneous replenishment in N ~~, either through very short τ_2 or large N_0 as in Fig. 8,~~ also fails to produce rapid LWP recovery (figures not shown).

4.2 Influence of Radiation

A comparison between results based on the simple radiation scheme (Stevens 2005) as opposed to RRTM shows a much stronger recovery in the RRTM simulation (c.f. Fig. 3a and 6b). As noted earlier, RRTM generates stronger longwave radiative cooling than the (untuned) simple calculation, which serves to support the contention that the slow recovery is related to the delay in TKE production by cloud radiative cooling. ~~Both the simple calculation and RRTM are based on plane-parallel radiative transfer. The simple calculation has been validated for overcast liquid phase clouds (Larson et al. 2007) but it is unclear how well it performs in broken open-cell scenes, such as during the initial hours of recovery, and if any biases exist between these two calculations in broken clouds. It is however clear that the recovery is sensitive to the method chosen for simulating radiative cooling. Whether 3-dimensional radiative transfer might also have an influence is speculative.~~

To explore the influence of radiation further, we consider the representation in RRTM of the effective free tropospheric air above the domain top. In the RRTM simulations thus far (Fig. 6b,c), the upper tropospheric humidity is maintained constant at the value at the domain top (≈ 2 g kg^{-1}). An additional ~~experiment~~ simulation in which the effective free tropospheric humidity is reduced to 0.01 g kg^{-1} is repeated. This would indicate a more efficient cooling of the system, e.g., in the absence of free tropospheric clouds. Note that this value only pertains to the effective radiative layer *above the model top* and does not directly affect the thermodynamics within the model domain. (Simulations with varying modeled free tropospheric air are shown in Fig. 6d.) As shown in Fig. ~~11~~12, the more efficient cooling associated with this drier effective free troposphere generates significantly stronger turbulence and a more rapid recovery to the closed cell state. Towards the end of the simulation this recovery of LWP is modulated to some extent by the stronger entrainment associated with the higher TKE – compounded by the solar absorption – so that LWP increases are small.

For perspective, Fig. ~~11~~ 12 also includes comparison with the control simulation (simple longwave radiation and standard N replenishment timescale of ~~2h~~2 h, with the time axis shifted so that the perturbations to N coincide) and the standard RRTM simulation but with a replenishment timescale of 10 h. We note that the rate of recovery of N is clearly an important factor in recovery of the LWP and the closed cell state. Also of interest is that z_i is larger and rebounds more rapidly in the Control case (simple longwave radiation) than in the RRTM-based simulations. Closer inspection shows that for the same N perturbation, the Control simulation generates less surface precipitation than does the RRTM simulation (Fig. ~~12~~13). The weaker thermodynamic stabilization in the Control simulation allows for a deepening boundary layer. Nevertheless, the deeper boundary layer by itself is not able to sustain a deeper cloud during the recovery because the weaker radiative cooling limits the regeneration of condensate. The RRTM simulation is characterized by significantly more positive vertical velocity skewness, and stronger ~~liquid water~~ q_t flux. Thus while the boundary layer is on average poorly mixed, the stronger updrafts supply moisture to the top of the boundary layer~~that helps maintain a higher~~, that help to boost f_c ~~, LWP, and TKE~~and LWP.

The influence of absorption of solar radiation on cloud recovery (Fig. 6c and Fig. ~~11~~12) is clearly manifested in both the initial stages after introduction of particles and towards the end of the simulations when LWP decreases markedly. The timing of the reintroduction of particles to the system relative to the diurnal cycle must therefore be considered to be a fundamental aspect of recovery. This point has also been raised in other modeling ~~studies~~ (Wang and Feingold, 2009b; Wang et al. 2011) and ~~observations~~ observational studies (Burleyson and Yuter, 2014).

4.3 Influence of Boundary Layer Depth

The DYCOMS-II RF02 boundary layer has a tendency to deepen steadily over the course of the simulation (Fig. 5). We now consider possible influence of the boundary layer depth on open-closed cell recovery. To address this, we simulate the system described in Fig. 3, but delay the application of the perturbation in $N(t)$ until 11 h, i.e., 8 h later than the standard simulation, when the boundary layer is deeper. In all other respects the perturbation is the same. This result is shown as the ~~dotted~~ dashed curve in Fig. ~~13~~14, shifted by t - 8 h. Clearly, recovery to the closed cell state is very similar to that for the shallower boundary layer. However, this result cannot be generalized since boundary layer depth is one of many factors determining cloud amount. The delayed N perturbation simulation generates a higher z_i throughout the simulation commensurate with the higher TKE. However, curiously LWP is lower prior to the precipitation and very close to the Control simulation thereafter so that radiative cooling is similar during the recovery stage. We have argued that recovery is closely related to the ability of the system to regenerate cloud water and radiative cooling. Why is recovery in the delayed perturbation case so similar to the Control case when the same LWP has to drive circulations over a deeper boundary layer? Analysis shows that the delayed perturbation simulation produces less surface rain R (both in rate and areal cover), and less thermodynamic stabilization, thus allowing the system to recover more readily (figures not shown). A more rigorous evaluation of recovery in deeper boundary layers such as those observed in the Southeast Pacific (Wood et al., 2011) is left to later study.

4.4 Mean vs Standard Deviation of LWP Phase Diagrams

While the asymmetry in the closed-open-closed cell transitions shows up clearly in the LWP and TKE time series, the system also displays asymmetry in other temporal evolution aspects. Considering parameterization applications, Yamaguchi and Feingold (2015) examined the domain mean LWP (μ(LWP)) vs. domain standard deviation of LWP (σ(LWP)) and showed that for the same case (and model) described here, the closed to open cell system follows a fairly predictable path from high

μ(LWP), low σ(LWP) in the closed-cell state, towards lower μ(LWP), high σ(LWP) in the open-cell state. Similar analysis is repeated here for the closed-open-closed transition for a number of different simulations, with and without a diurnal solar cycle and with variations in the subsidence and free tropospheric humidity. One illustrative example associated with Fig. 7 is shown in Fig. ~~14~~ 15 but all exhibit similar features. First, the simulations all show similar phase paths as in Yamaguchi and Feingold (2015) for the closed-open transition. Of note is that for a given μ(LWP) the open-closed transition is characterized in all cases by higher σ(LWP) than for the closed-open transition. The higher σ(LWP) on the open-closed path is an expression of the slow recovery; i.e., the low cloudiness (high variance) state attempting to achieve a more cloudy (lower variance) state (see also Fig. 2).

5 Summary

This work is motivated by the radiative impacts of the large ~~increase~~ difference in the amount of solar radiation absorbed at the Earth's surface in open vs. closed cellular convection, and a desire to (i) understand the propensity of cellular systems to transition back and forth between states, and (ii) elucidate key processes controlling the transitions. Satellite imagery often shows ship track effluent closing open cells, and yet cloud resolving models that include different levels of complexity in the representation of the aerosol lifecycle produce more ambiguous results regarding the ability of aerosol perturbations to fill in open cells (Wang and Feingold 2009b; Wang et al. 2011; Berner et al. 2013). Rather than include detailed representation of aerosol processes as in Kazil et al. (2014), we have elected to prescribe a simple symmetrical time series of the drop concentration evolution $N(t)$. Even this symmetrical $N(t)$ does not produce a symmetrical LWP(t) suggesting that some underlying system behavior is responsible for the relatively slow recovery. The key results of this study can be ~~encapsulated~~ recapitulated as follows.

1. In stratocumulus clouds driven by cloud-top radiative cooling, changes in LWP precede changes in TKE. Once in the open cell state, the recovery of the system depends on regeneration of LWP and attendant radiative cooling; thus the lag in TKE ~~build up~~ build-up represents a barrier to recovery. Although injection of aerosol into the system helps suppress precipitation and generate LWP, until N is large enough, the increasing LWP also helps generate precipitation, representing further barrier to recovery. Thus while a recharge of N is a necessary condition for recovery from the open cell state, it cannot explain the basic asymmetry in the recovery.

2. The relatively slow open-closed transition is related to the stabilization caused by the rain during the low N open-cell state and the relatively long time it takes for a build up in the TKE after the reintroduction of N. The recovery is slower when longwave cooling is countered by shortwave absorption (Fig. 6c), for large imposed reductions in N (Figs. 3, 4, 6), and when the rate of reintroduction of N is slow (Fig. ~~11~~12) or the amount too small (Wang et al. 2011).

Cloud layers within the free troposphere would also reduce the effectiveness of longwave cooling and delay recovery (Fig. ~~11). Recovery would be more rapid if stronger surface fluxes were~~ 12).

3. A region of sub-cloud buoyancy consumption of TKE during the recovery from open-to-closed cells has been identified (Fig. 8b). Examination of a sample of the simulations presented herein show that the extent, magnitude, and persistence of this area is proportional to the amount of rain generated during the open-cell phase. Recovery to the closed-cell state proceeds once this barrier has been removed and surface moisture can be transported more effectively to the cloud (Fig. 8c). For example, recovery is more rapid when stronger surface latent and sensible heat fluxes are coincident with the replenishment of N (Fig. ~~9).~~ 10). In this case, the region of buoyancy consumption of TKE is significantly reduced and surface vapor can reach the cloud layer more readily.

4. In the predator-prey model, asymmetry is a fundamental property of the equations because they include delay terms. It is shown that the degree of the asymmetry is controlled by the timescale for replenishment of H, i.e., τ_1 (or alternatively H_0; Eq. 1) after recovery from the open cell state. Simple tests with either small τ_1 or large H_0, i.e., strong meteorological forcing accompanying the injection of aerosol, result in ~~much~~ more symmetric transitions.

These results shed light on why the transition from open to closed cellular state can be significantly more difficult than the reverse, and point to the need to understand the meteorological, radiative, and surface flux environment in which these transitions occur. Transitions from the open to the closed cellular state are expected to be slower during the daytime, when the free troposphere is cloudier (Fig. ~~11~~12), and when aerosol perturbation/replenishment is slow (Fig. ~~11~~12). Aspects of this hypothesis can be tested with satellite observations and reanalysis.

Appendix A:

Sensitivity to Grid ~~Size~~Spacing

The standard simulations are all performed on a relatively coarse grid spacing of $\Delta x \times \Delta y \times \Delta z$ = 200 m $\times$ 200 m $\times$ 10 m (aspect ratio of 20:1). Before embarking on the more extensive simulations presented here, system response was explored for finer grids and smaller aspect ratios: $\Delta x \times \Delta y \times \Delta z$ = 100 m $\times$ 100 m $\times$ 10 m (aspect ratio of 10:1); and 75 m $\times$ 75 m $\times$ 10 m (aspect ratio of 7.5:1). All simulations were performed on the same domain size (40 km). Figure A1 compares the LWP, TKE, f_c and z_i time series for these three configurations and shows that the characteristic behavior of these simulations is similar. The finer grid simulations tend to generate more vigorous and deeper boundary layers. Rates of recovery of LWP and f_c are similar. While it would be desirable perhaps to perform all simulations at higher resolution and smaller aspect ratios, Fig. A1 suggests that the key aspects of the system response are robust to grid ~~size~~spacing.

Acknowledgements. GF, TY and JK are funded by NOAA's Climate Goal and the Department of Energy's Atmospheric Science Program. IK is funded by the European Research Council under the European Union's Seventh Framework Programme (FP7/2007-2013)/ERC Grant agreement number [306965]. The authors are most grateful to Marat Khairoutdinov for sharing his System for Atmospheric Modeling and to Peter Blossey for his help with the RRTM code integration.

References

Ackerman, A. S., vanZanten, M. C., Stevens, B., Savic-Jovcic, V., Bretherton, C. S., Chlond, A., Golaz, J.-C., Jiang, H., Khairoutdinov, M., Krueger, S. K., Lewellen, D. C., Lock, A., Moeng, C.-H., Nakamura, K., Petters, M. D., Snider, J. R., Weinbrecht, S., and Zulauf, M.: Large-eddy simulations of a drizzling, stratocumulus-topped marine boundary layer, Mon. Weather. Rev., 137, 1083 – 1110, 2009.

Berner, A. H., Bretherton, C. S., Wood, R., and Muhlbauer, A.: Marine boundary layer cloud regimes and POC formation in a CRM coupled to a bulk aerosol scheme, Atmos. Chem. Phys., 13, 12549 – 12572, doi:10.5194/acp-13-12549-2013, 2013.

Burleyson, C. D. and Yuter, S. E.: ~~Sub-diurnal~~ Subdiurnal stratocumulus cloud fraction variability and sensitivity to precipitation. J.Climate, ~~conditionally accepted,~~ 28, 2968 – 2985, DOI: 10.1175/JCLI-D-14-00648.1, 2015.

Cavallo, S. M., J. Dudhia, and Snyder, C.: A multilayer upper-boundary condition for longwave radiative flux to correct temperature biases in a mesoscale model. Mon. Wea. Rev., 139, 1952-1959, 2010.

Feingold, G., S. M. Kreidenweis, B. Stevens, and Cotton, W. R.: Numerical simulation of stratocumulus processing of cloud condensation nuclei through collision-coalescence. J. Geophys. Res, 101, 21,391–21,402, 1996.

Feingold, G., I. Koren, H. Wang, H. Xue, and Brewer, W. A.: Precipitation-generated oscillations in open cellular cloud fields. Nature, 466, doi:10.1038 / nature09314, 2010.

Feingold, G. and Koren, I.: A model of coupled oscillators applied to the aerosol-cloud- precipitation system, Nonlinear Proc. Geoph., 20, 1011 – 1021, 2013.

Goren, T. and Rosenfeld, D.: Satellite observations of ship emission induced transitions from broken to closed cell marine stratocumulus over large areas, J. Geophys. Res., 117, D17206, doi:10.1029/2012JD017981, 2012.

Jiang, Q., and Wang, S.: Aerosol Replenishment and Cloud Morphology: A VOCALS Example. J. Atmos. Sci., 71, 300 – 311. doi: http://dx.doi.org/10.1175/JAS-D-13-0128.1, 2014

Kazil, J., Wang, H., Feingold, G., Clarke, A. D., Snider, J. R., and Bandy, A. R.: Modeling chemical and aerosol processes in the transition from closed to open cells during VOCALS-REx, Atmos. Chem. Phys., 11, 7491 – 7514, doi:10.5194/acp-11-7491- 2011, 2011.

Kazil, J., G. Feingold, H. Wang, and Yamaguchi, T.: On the interaction between marine boundary layer cellular cloudiness and surface heat fluxes. Atmos. Chem. Phys., 14, 61–79, doi:10.5194/acp-14-61-2014, 2014.

Khairoutdinov, M. F., and Kogan, Y. L.: A new cloud physics parameterization in a large-eddy simulation model of marine stratocumulus. Mon. Wea. Rev., 128, 229 – 243, 2000.

Khairoutdinov, M. F. and Randall, D. A.: Cloud resolving modeling of the ARM summer 1997 IOP: model formulation, results, uncertainties, and sensitivities, J. Atmos. Sci., 60, 607 – 625, 2003.

Koren, I., and Feingold, G.: The aerosol-cloud-precipitation system as a predator-prey problem. Proc. Nat. Acad. Sci., 10.1073/pnas.1101777108, 2011.

Koren, I., and Feingold, G.: Adaptive behavior of marine cellular clouds. Nature Sci. Rep., 3, 2507; DOI:10.1038/srep02507, 2013.

Larson, V. E., K. E. Kotenberg, and Wood, N. B.: An Analytic Longwave Radiation Formula for Liquid Layer Clouds. Monthly Wea. Rev., 135, 689 – 699, DOI: 10.1175/MWR3315.1, 2007.

Mechem, D. B., Yuter, S. E., and De Szoeke, S. P.: Thermodynamic and aerosol controls in southeast Pacific stratocumulus, J. Atmos. Sci., 69, 1250 – 1266, 2012.

Mlawer, E. J., S. J. Taubman, P. D. Brown, M. J. Iacono, and Clough, S. A.: Radiative transfer for inhomogeneous atmospheres: RRTM, a validated correlated-k model for the longwave. J. Geophys. Res., 102(D14), 16663 – 16682, 1997.

Moeng, C.-H. : Large eddy simulation of a stratus-topped boundary layer. Part II. Implications for mixed layer modeling. J. Atmos. Sci., 44, 1605–1614.

Pawlowska, H., and Brenguier, J. L.: An observational study of drizzle formation in stratocumulus clouds for general circulation model (GCM) parameterizations. J. Geophys. Res., 108, 8630, doi:10.1029/2002JD002679, 2003.

Savic-Jovcic, V. and Stevens, B.: The structure and mesoscale organization of precipitating stratocumulus, J. Atmos. Sci., 65, 1587 – 1605, 2008.

Sharon, T. M., Albrecht, B. A., Jonsson, H. H., Minnis, P., Khaiyer, M. M., van Reken, T. M., Seinfeld, J., and Flagan, R.: Aerosol and cloud microphysical characteristics of rifts and gradients in maritime stratocumulus clouds, J. Atmos. Sci., 63, 983 – 997, 2006.

Stevens, B., W. R. Cotton, G. Feingold, and Moeng, C.-H.: Large-eddy simulations of strongly precipitating, shallow, stratocumulus-topped boundary layers. J. Atmos. Sci., 55, 3616–3638, 1998.

Stevens, B., Vali, G., Comstock, K., Wood, R., Van Zanten, M. C., Austin, P. H., Bretherton, C. S., and Lenschow, D. H.: Pockets of open cells and drizzle in marine stratocumulus, B. Am. Meteorol. Soc., 86, 51 – 57, 2005.

Wang H., and Feingold, G.: Modeling mesoscale cellular structures and drizzle in marine stratocumulus. Part I: Impact of drizzle on the formation and evolution of open cells. J. Atmos. Sci., 66, 3237 – 3256, 2009.

Wang H., and Feingold, G.: Modeling mesoscale cellular structure and drizzle in marine stratocumulus. Part II: The microphysics and dynamics of the boundary region between open and closed cells. J. Atmos. Sci., 66, 3257 – 3275, 2009..

Wang, H., P. J. Rasch, and Feingold, G.: Manipulating marine stratocumulus cloud amount and albedo: a process-modelling study of aerosol-cloud-precipitation interactions in response to injection of cloud condensation nuclei. Atmos. Chem. Phys.,11, 4237 – 4249, 2011.

Wood, R., and Hartmann D. L. Spatial variability of liquid water path in marine low cloud: The importance of mesoscale cellular convection. J. Climate, 19, 1748 – 1764, 2006.

Wood, R., Mechoso, C. R., Bretherton, C. S., Weller, R. A., Huebert, B., Straneo, F., Albrecht, B. A., Coe, H., Allen, G., Vaughan, G., Daum, P., Fairall, C., Chand, D., Gallardo Klenner, L., Garreaud, R., Grados, C., Covert, D. S., Bates, T. S., Krejci, R., Russell, L. M., de Szoeke, S., Brewer, A., Yuter, S. E., Springston, S. R., Chaigneau, A., Toniazzo, T., Minnis, P., Palikonda, R., Abel, S. J., Brown, W. O. J., Williams, S., Fochesatto, J., Brioude, J., and Bower, K. N.: The VAMOS Ocean-Cloud-Atmosphere- Land Study Regional Experiment (VOCALS-REx): goals, ~~plat- forms~~platforms, and field operations, Atmos. Chem. Phys., 11, 627 – 654, doi:10.5194/acp-11-627-2011, 2011.

Xue, H., and Feingold, G.: Large eddy simulations of trade-wind cumuli: Investigation of aerosol indirect effects. J. Atmos. Sci., 63, 1605 – 1622, 2006.

Xue, H., Feingold, G., and Stevens, B.: Aerosol effects on clouds, precipitation, and the organization of shallow cumulus convection, J. Atmos. Sci., 65, 392 – 406, 2008.

Yamaguchi, T., D. A. Randall, and Khairoutdinov, M. F.: Cloud modeling tests of the ULTIMATE-MACHO scalar advection scheme. Mon. Wea. Rev., 139, 3248 – 3264, 2011.

Yamaguchi, T. and Feingold, G.: On the relationship between open cellular convective cloud patterns and the spatial distribution of precipitation. Atmos. Chem. Phys. 15, 1237 – 1251, 2015.

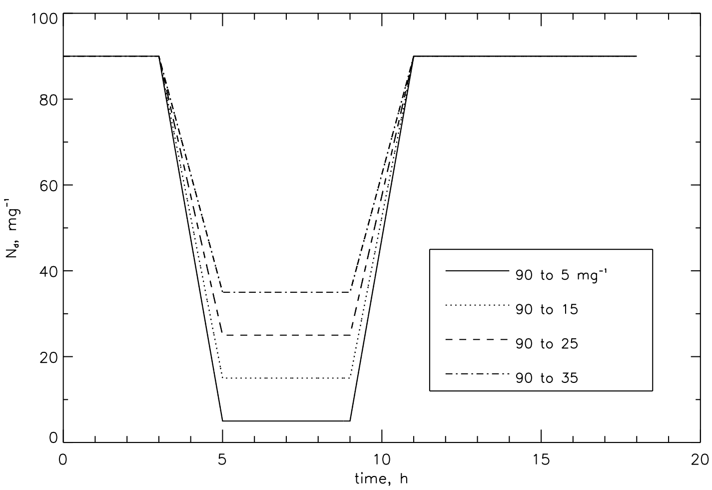

Figure 1. Time series of imposed time series of drop concentration N. The minimum N is varied between 5 mg^{-1} and 35 mg^{-1}.

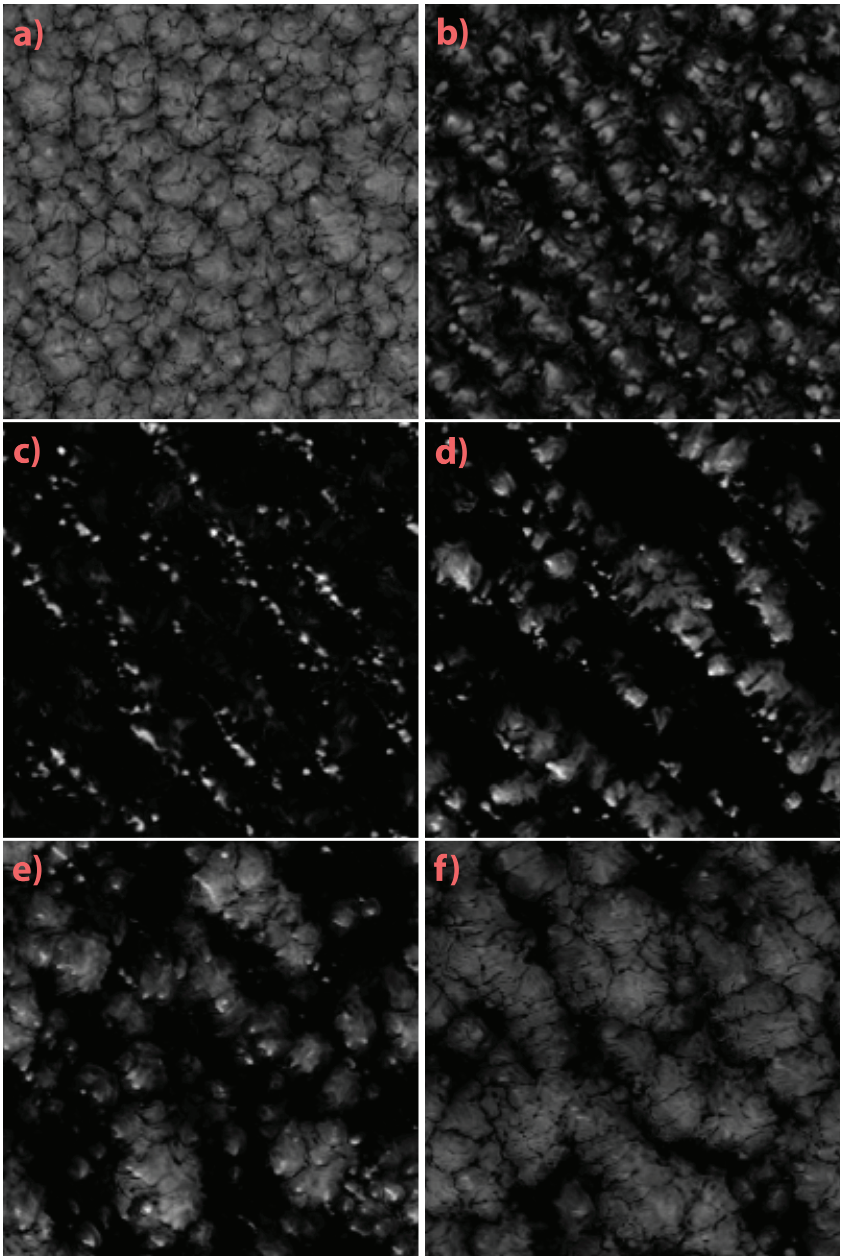

Figure 2. LWP at t = (a) 3 h (closed cell), (b) ~~5h~~ 5 h (closed transitioning to open), (c) 7 h (open cell), (d) 11 h (open transitioning to closed), (e) 13 h (further recovery to closed), (f) 18 h (closed cell). Control simulation with minimum N = 5 mg^{-1}. The grey scale ranges from 0 to 450 g m^{-2}.

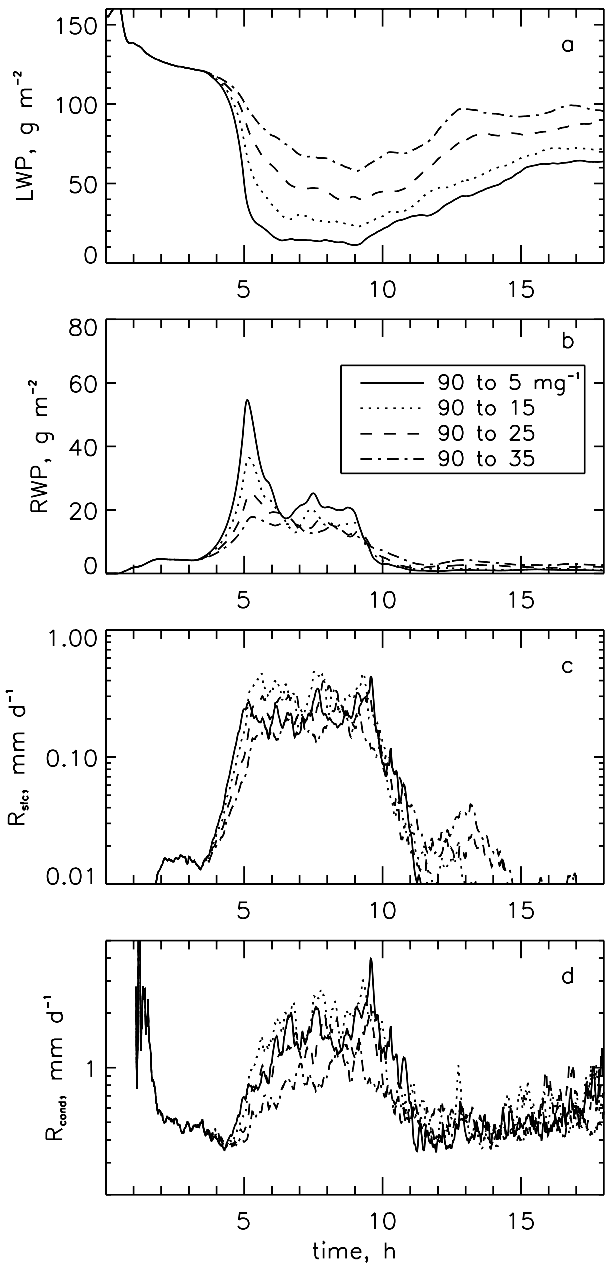

Figure 3. Time series of (a) LWP, (b) Rain Water Path (RWP), ~~and~~ (c) domain mean surface rain rate ~~R~~ R_{sfc}, and (d) surface rain rate conditionally sampled for $R \geq 0.1$ mm d^{-1} (R_{cond}) for the control case, and for the various minimum N as in Fig. 1. Recovery becomes progressively more difficult with decreasing minimum N. The initial spike in surface R_{cond} is related to the fact that during the first hour of simulation, collision-coalescence and sedimentation are not simulated.

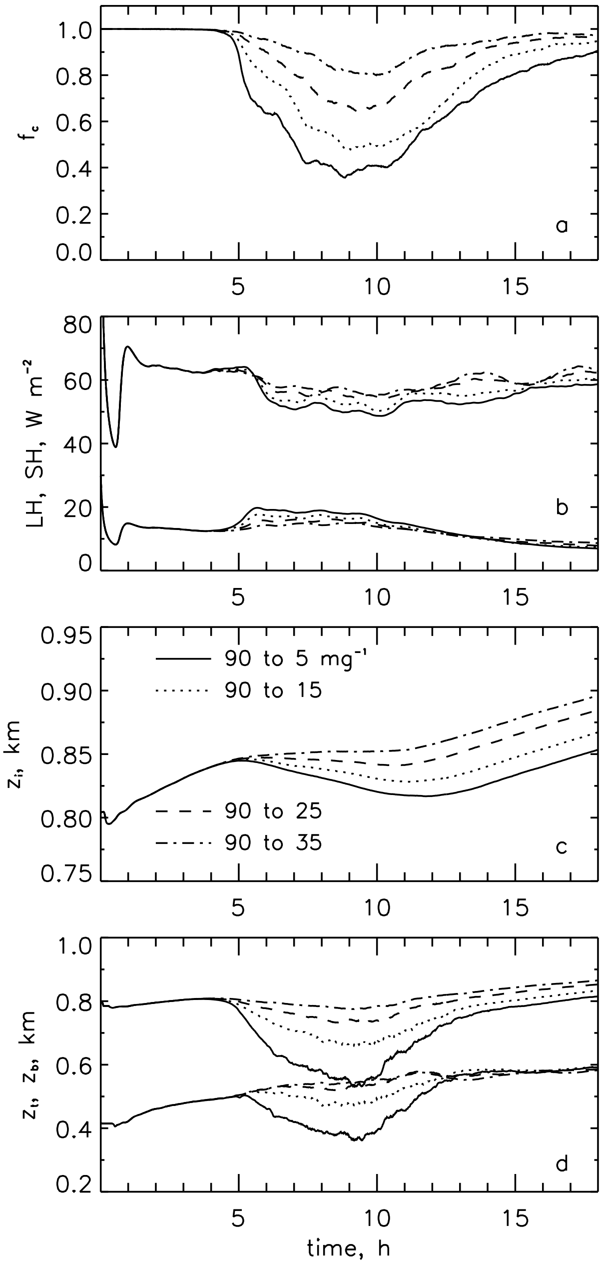

Figure 4. Time series of (a) cloud fraction f_c, (b) surface Latent and Sensible Heat fluxes (LH and SH, respectively; LH $>$ SH), (c) inversion height z_i, and (d) cloud top z_t and cloud base z_b for the control case and the various minimum N as in Fig. 1. Note the suppression of the deepening of the boundary layer associated with drizzle.

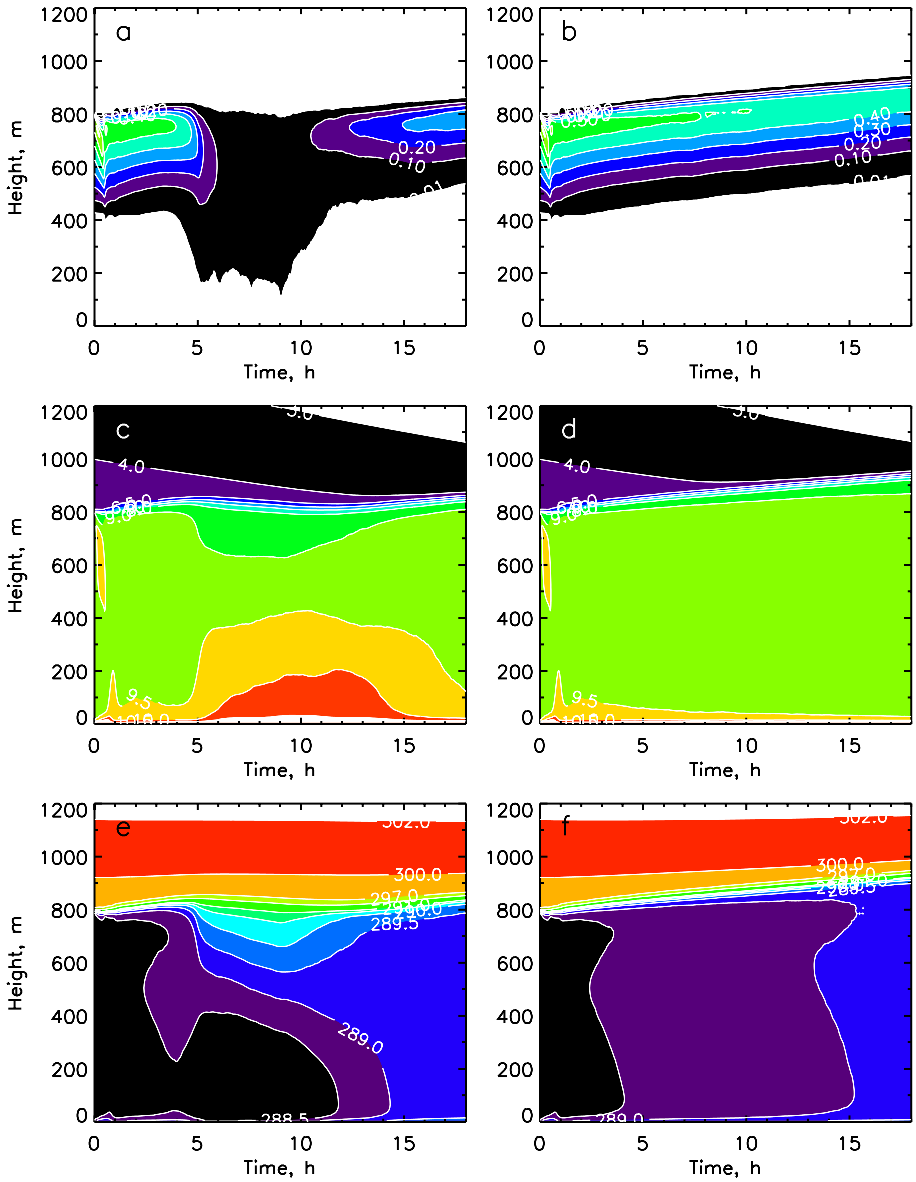

Figure 5. Domain average profiles of (a) and (b) liquid water ~~content~~ mixing ratio q_c, (c) and (d) total water mixing ratio q_t, and (e) and (f) liquid water potential temperature θ_l. Left column: control case with minimum N = 5 mg^{-1}; Right column: N = 90 mg^{-1} throughout the simulation. Drizzle results in a drying of the cloud layer and a moistening of the surface (c). The drizzling period is characterized by poor ~~domain~~ average vertical mixing. The drizzling system eventually recovers to a well-mixed state, although surface moisture persists.

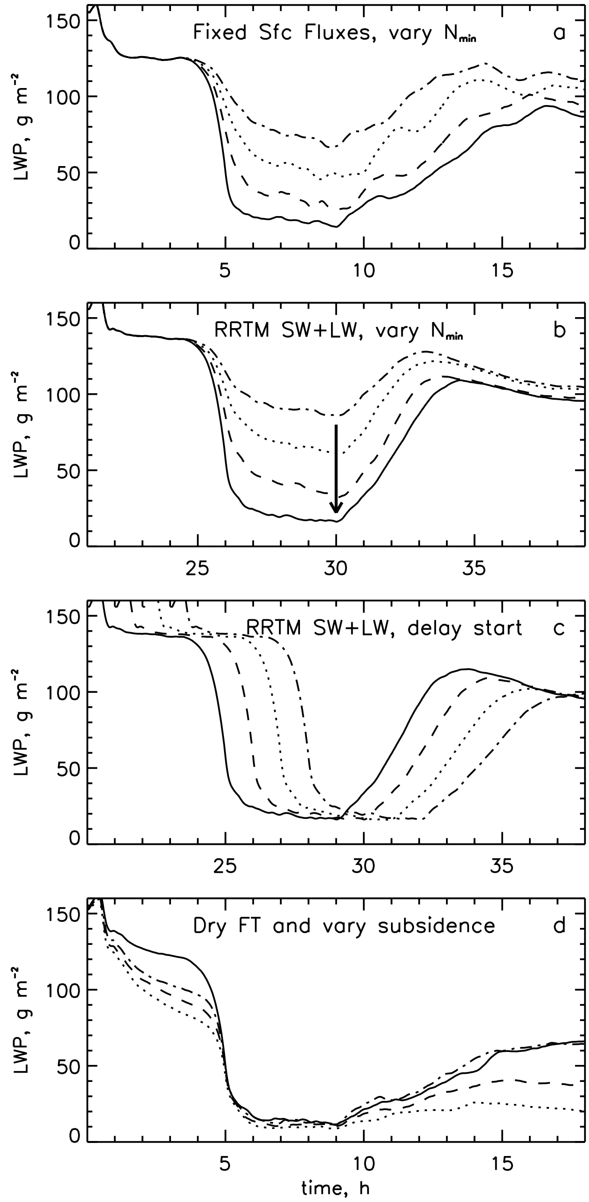

Figure 6. Tests of robustness of LWP recovery. (a) Control case but with fixed surface fluxes and no winds. Line types as in Fig. 1; (b) RRTM (shortwave and longwave) and start time of 21:00 LT. Line types as in Fig. 1. The arrow points to sunrise at 06:00 LT (t = 30 h); (c) as in (b) but with start times staggered by 1 h between 20:00 LT and 23:00 LT; (d) Control case (solid line), Dry air aloft (dashed line), dry air aloft and divergence increased to 5 $\times$ 10^{-6} s^{-1} (dotted line), and dry air aloft but divergence decreased to 1 $\times$ 10^{-6} s^{-1} (dash-dotted line). The drier air aloft is calculated according to ~~$q_v = q_{v,0} - 3[1 - exp((795 - z)/500)]$~~ $q_v = q_{v,0}$ - 3 g kg^{-1} [1 - exp((795 - z) / 500)] with $q_{v,0}$ = 3 g kg^{-1} rather than $q_{v,0}$ = 5 g kg^{-1} in the control case. (Terms in the exponent are in meters.) The precipitable water at t = 0 is 10.0 mm, compared to 11.7 mm for the standard profile. In (c) and (d) the minimum N = 5 mg^{-1}.

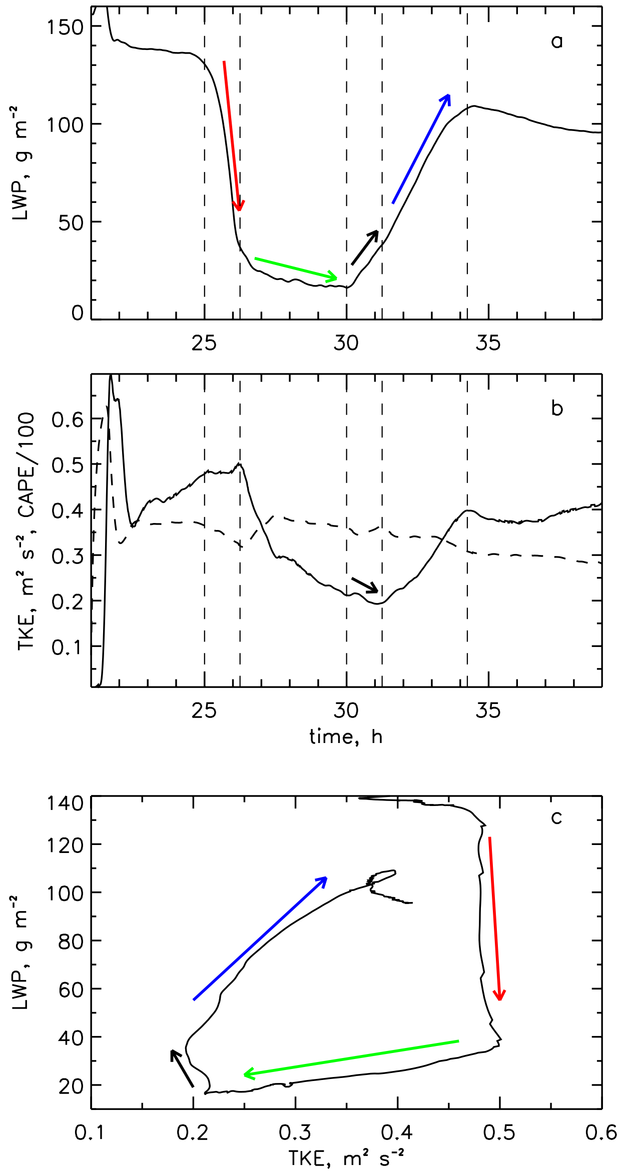

Figure 7. Analysis of RRTM simulation and minimum N = 5 mg^{-1} (solid line, Fig. 6b). Time series of (a) domain mean LWP and (b) ~~domain~~ TKE, averaged horizontally, and over the boundary-layer ~~average TKE~~ depth, (solid line) and CAPE (dashed line); (c) a phase diagram of (a) vs. (b). Colored arrows indicate stages of evolution of the system. Vertical dashed lines are included to focus on temporal phase lags between LWP and TKE. Red arrow: LWP falls rapidly while TKE continues to increase; Green arrow: both LWP and TKE decrease; Black arrow: LWP begins to recover while TKE still decreases; Blue arrow: LWP and TKE increase in unison as the closed cell state recovers.

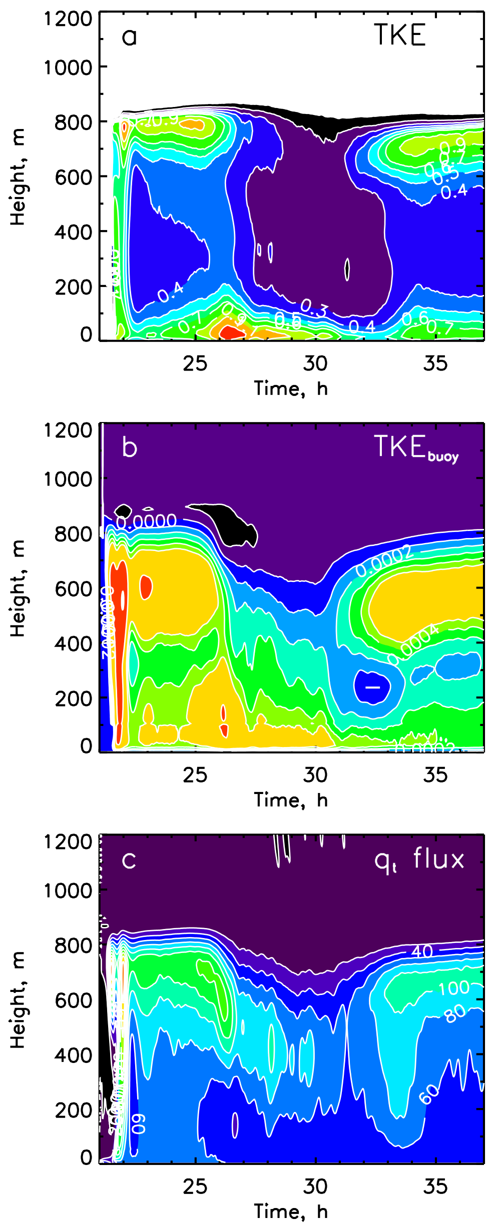

Figure 8. Time-height cross sections associated with Fig. 7: (a) resolved TKE (m^2s^{-2}), (b) buoyancy production of TKE (m^2s^{-3}), and (c) q_t flux (W m^{-2}). Note how in (a), the peak TKE transitions from the cloud layer to the surface during closed-to-open cell transition (t ≈ 26 h) and back to the cloud layer upon recovery. In (b), an area of negative buoyancy production of TKE (consumption) is indicated by a white minus

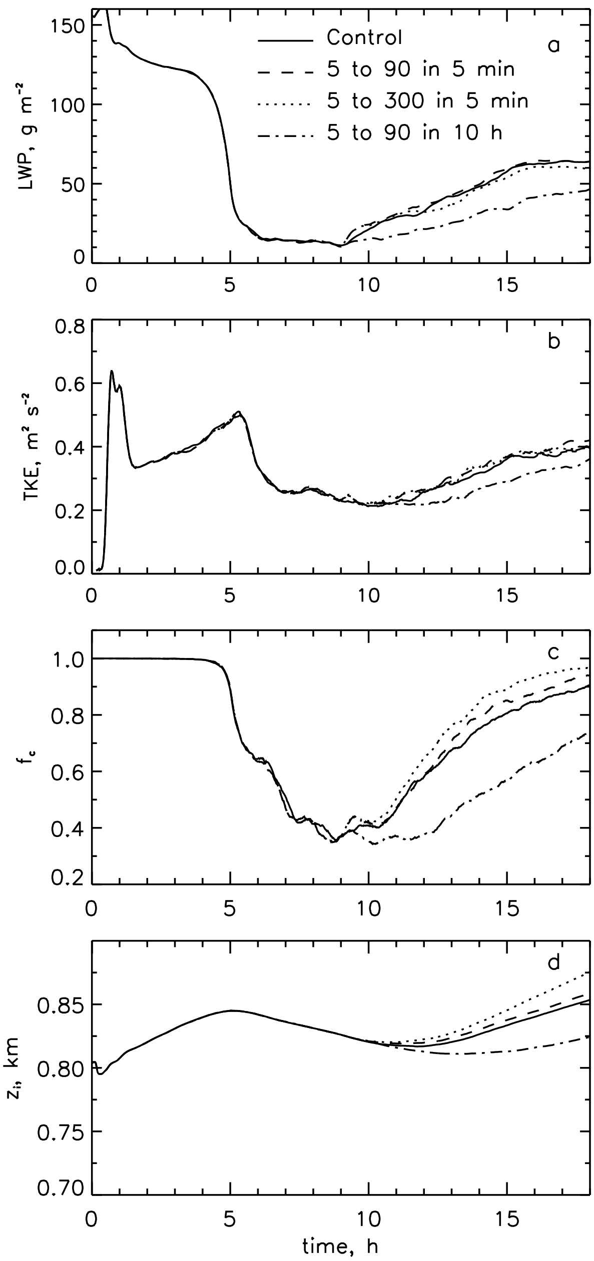

Figure 9. Simulations testing the importance of N for recovery of the closed cell state for Control case set up with variations. Simulations prior to t = 9h are the same (slight differences are due to different machine compilers and processors). After t = 9h, N increases to 90 mg $^{-1}$ within 2 h as in Fig. 1 (solid line, Control); N recovers to 90 mg^{-1} within 5 min (dashed line); N recovers to 300 mg^{-1} within 5 min (dotted line); and N recovers to 90 mg^{-1} within 10 h (dash-dotted line).

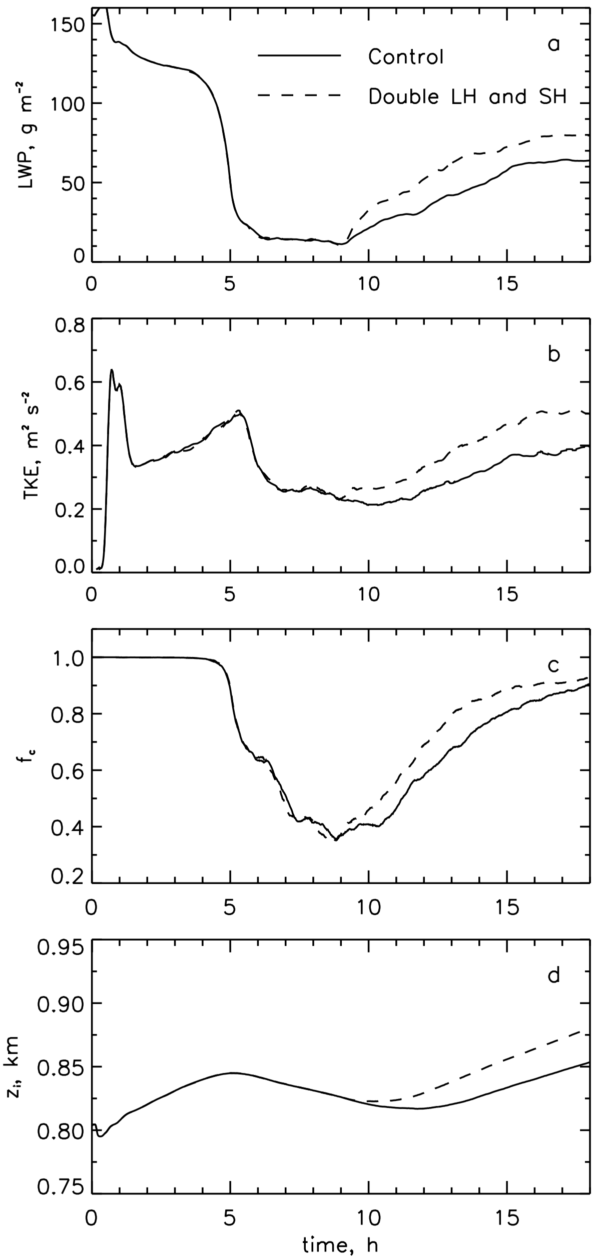

Figure 10. Simulations considering the influence of surface forcing on recovery. Soild line: Control simulation; Dashed line: latent and sensible heat fluxes are double their interactively calculated values after t = ~~9h~~9 h, i.e., concurrent with the increase in N.

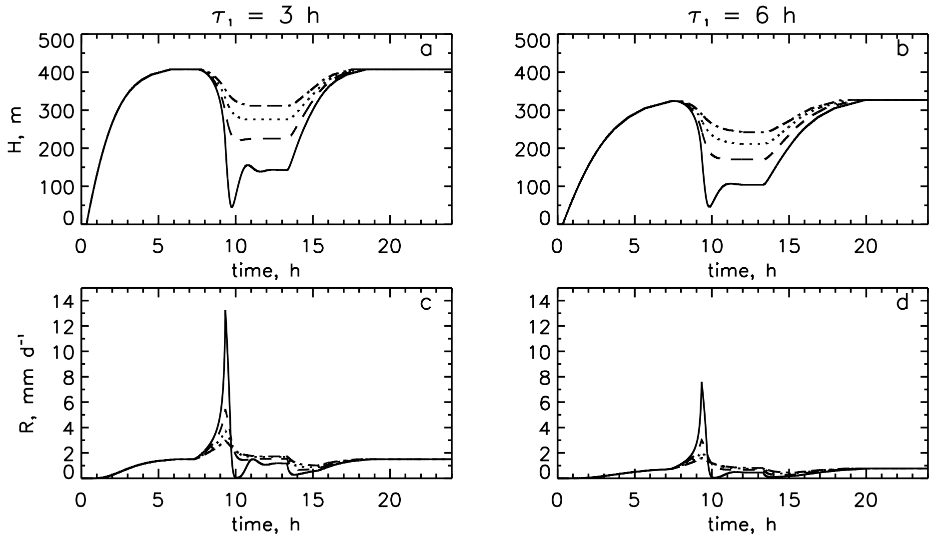

Figure 11. Predator-Prey analog to the cloud system (Eqns. ~~(~~1 ~~)~~ and ~~(~~3)~~and with~~ . $N(t)$ is prescribed as in Fig. 1 but the ~~Figure)~~timing is 4 h later to allow for predator-prey model spin-up. Model parameters are H_0 = 650 m, T = 20 min. ~~(a) Meteorological carrying capacity or~~ Left column: H and R solutions for H recovery time τ_1 = 3 h; ~~and (b)~~ Right column: H ~~recovery time~~ and R solutions for τ_1 = ~~0.5~~ 6 h. ~~Solid line represents H and dashed line represents R~~Line types represent the various N time series (as in Fig. 1, but with N in cm^{-3}). In both cases the concurrence of rapid increase in R during the rapid reduction in LWP is simulated as in Fig. 3ab. Smaller values of ~~τ_1~~ N perturbation exhibit ~~rapid cloud depth or "meteorological"~~ faster H recovery ~~and quicker transition to~~ after reintroduction of N. Recovery is also faster in the ~~closed cell state~~case of smaller τ_1. ~~By analogy, c.f. simulations with Control radiative forcing (Fig. 3a) and stronger (RRTM) radiative forcing (Fig. 6b).~~

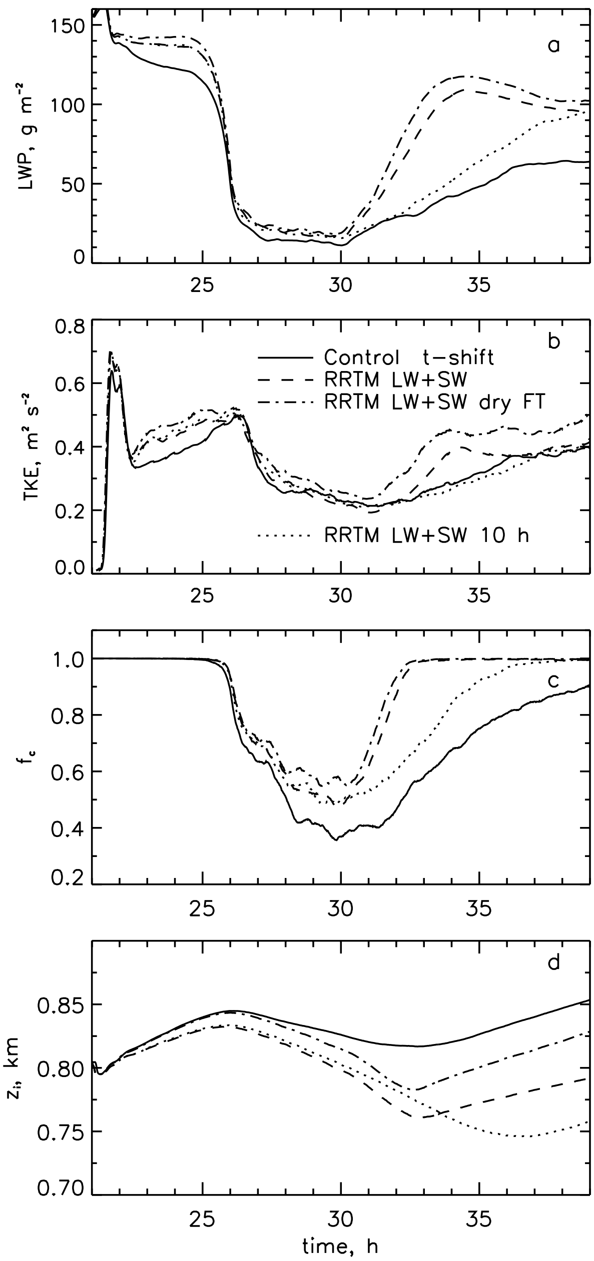

Figure 12. Perspective of different parameters controlling recovery. Solid line: Control simulation with time shift such that $N(t)$ time series coincide; Dashed line: RRTM simulation as in Fig. 6b; Dotted line: same as dashed line but with N recovering to 90 mg^{-1} over 10 h; Dash-dotted line: RRTM simulation as in Fig. 6b but with drier free troposphere imposed above model domain top. Minimum N = 5 mg^{-1} in all cases. Slow replenishment of N retards cloud recovery while stronger radiative forcing enhances recovery.

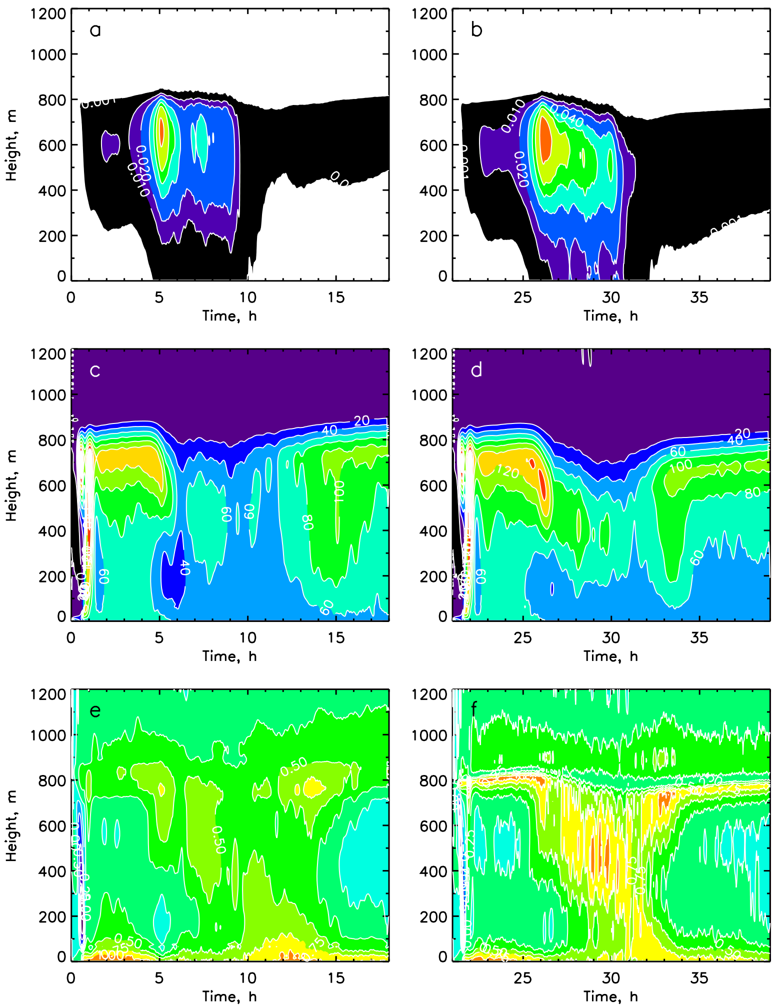

Figure 13. Domain average profiles of (a) and (b) rain water content q_r, (c) and (d) ~~liquid water~~ q_t flux, and (e) and (f) vertical velocity skewness. Left column: control case with minimum N = 5 mg^{-1}; Right column: RRTM simulation (dashed line in Fig. ~~11~~12). Stronger drizzle in the RRTM simulation generates stronger positive skewness and higher ~~liquid water~~ q_t flux during the open-cell period, which help maintain higher f_c ~~, LWP,~~ and ~~TKE~~ LWP (Fig. ~~11~~12). Contour intervals: ~~for~~ rain water content: 0.01~~to~~, 0.02, 0.04, 0.06, 0.08, 0.12, 0.18 g kg^{-1} ~~in increments of 0.01~~; ~~for liquid water~~ q_t flux: 20 to ~~140~~ 160 W m^{-2} in increments of 20; skewness: -1.5 to 1.5 in increments of 0.25. Color scales are identical for left and right columns.

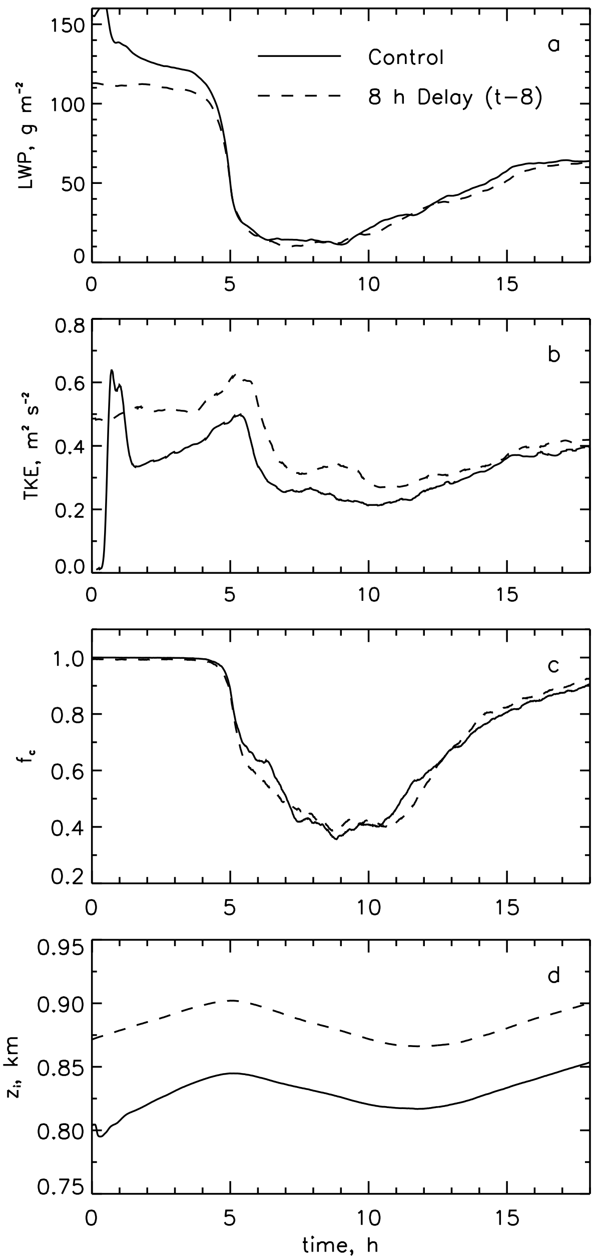

Figure 14. Investigation of importance of timing of N perturbation. Solid line: Control case; Dashed line: Control case but with N perturbation delayed by ~~8h~~ 8 h during which time the boundary layer has deepened (time axis shifted so N perturbation coincides). In both cases LWP and f_c recovery are similar. ~~Add some explanation of the higher TKE and deeper BL for similar (or even smaller LWP. WHY???)~~

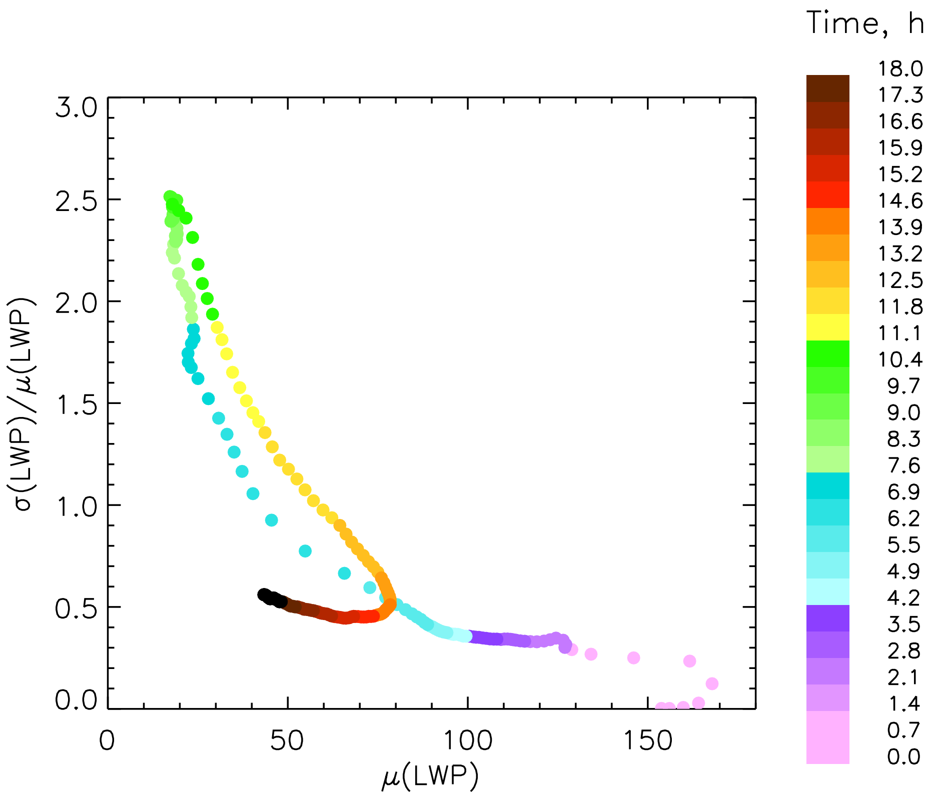

~~Phase diagram for the relative dispersion of LWP (σ (LWP)/μ(LWP)) vs. the mean LWP (μ(LWP)) for the simulation in Fig. 7. Note that the recovery from open to closed cell state is characterized by higher σ/μ.~~

Figure 15. Phase diagram for the relative dispersion of LWP (σ (LWP)/μ(LWP)) vs. the mean LWP (μ(LWP)) for the simulation in Fig. 7. Colors indicate simulation time. Note that the recovery from open to closed cell state is characterized by higher σ/μ for given μ.

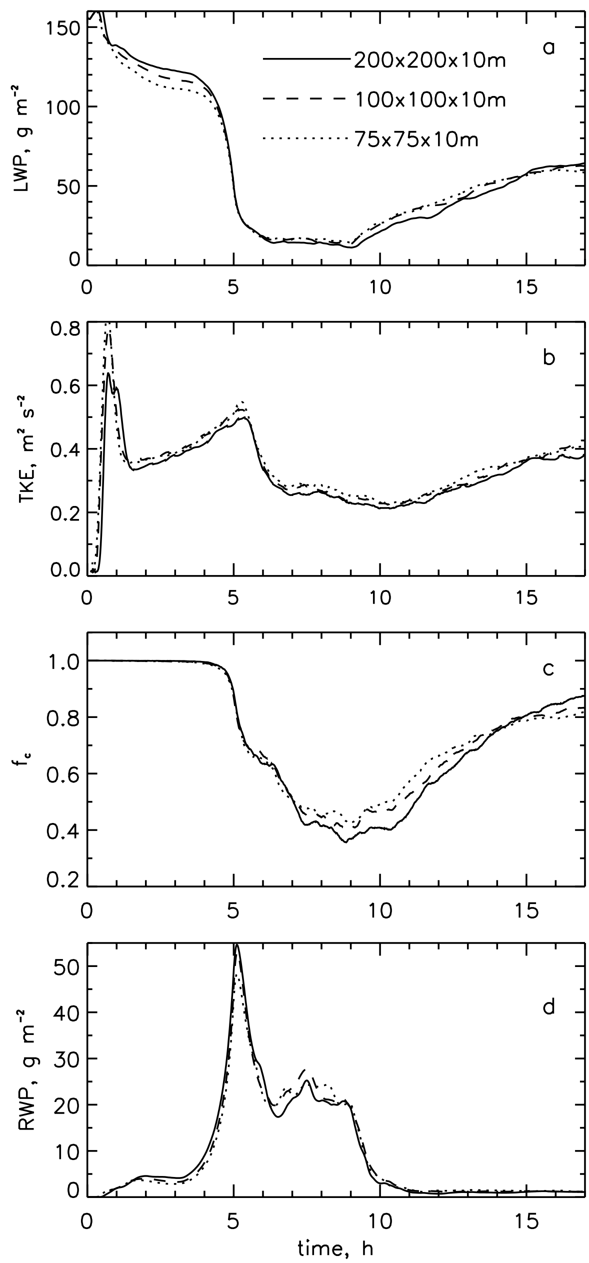

Figure A1. Sensitivity of results to grid ~~size~~spacing (meters).